Figure #	Figure title One sentence only	Filename This should be the name the file is saved as when it is uploaded to our system. Please include the file extension. i.e.: *Smith_ED_Fig1.jpg*	Figure Legend If you are citing a reference for the first time in these legends, please include all new references in the Online Methods References section, and carry on the numbering from the main References section of the paper.
Extended Data Fig. 1	Restriction activity and surface exposure of SERINC.	Extended_Data_Fig1_VEP.jpeg	**a**,**b**, HIV-1 restriction activity of *Dm*SERINC compared with human SERINC5 and SERINC2. Human and *Dm*SERINC proteins with HA tags at their C-termini were expressed in HEK293T cells with two different expression vectors (pcDNA and pBJ6) which provide high and low expression, respectively. Levels of the indicated SERINC proteins were assessed by Western blotting using an anti-HA antibody (uncropped blot images are shown in the Source Data) (**a**) and by flow cytometry (**b**) to detect the proteins surface expression (**b**, top) or total expression (**b**, bottom) using an anti-FLAG antibody on non-permeabilzed and permeabilized cells respectively. **c**, Effect of SERINC expression on infectivity of HIV-1 produced in HEK293T cells transfected to express the indicated SERINC-iFLAG-HA and Nef-deficient HIV-1_{NL4-3}. (Data shown are mean and s.d. of n=4 technical repeats. Data are provided in the Source Data). **d**, Insertion of the FLAG epitope into ECL4 does not interfere with the anti-HIV-1 restriction activity of SERINC5. Infectivity of Nef-deficient HIV-1_{NL4-3} produced in HEK293T cells transfected to express unmodified human SERINC5-HA or a variant modified by inserting a FLAG tag within its ECL4 (SERINC5-iFLAG-HA). Two different expression vectors (pcDNA and pBJ6) were used in order to obtain high and low SERINC5 expression as shown

			above (Data shown are mean and s.d. of n=4 technical repeats. Data are provided in the Source Data). **e**, Effect of ECL5 SERINC5 variants on HIV-1 susceptibility to neutralization. IC_{50} values derived from fitted sigmoidal curves shown in figure 4, obtained from quadruplicate repeats using antibodies 2F5 and 4E10 on Nef-defective HIV-1_{NL4-3} pseudotyped with the envelope glycoprotein derived from HIV-1_{JR-FL}, produced by transfecting HEK293T cells with the indicated PBJ5-SERINC5-iFLAG-HA variants or the empty vector control (Data shown are mean and 95% confidence interval of n=4 technical repeats. Data are provided in the Source Data).
Extended Data Fig. 2	Human SERINC5 purification and EM	Extended_Data_Fig2_VEP.jpeg	**a**, Size exclusion chromatography profile. **b**, Left: SDS-PAGE analysis of resulting fractions; right: cleavage of TwinStrep tag and deglycosylation (uncropped gel images are shown in the Source Data). **c**, Sample micrograph of negatively stained particles. **d**, Representative 2D class averages. **e**, Schematic of image processing and reconstruction of the human SERINC5 cryo-EM structure. Details are given in Extended Methods. **f**, Left: Gold standard FSC curve for the cryo-EM reconstruction of SERINC5, Right: Euler angle distribution plot for particles included in the final 3D reconstruction; 3DFCS reports a sphericity of 0.976. **g**, The map colored according to local resolution estimated with blocres.
Extended Data Fig. 3	*Dm*SERINC purification and EM.	Extended_Data_Fig3_VEP.jpeg	**a**, Left: chromatography profile of *Dm*SERINC on a Superdex 200 column; the blue arrow highlights elution of the material, which was re-injected onto the column. Right: elution profile of hexameric *Dm*SERINC. **b**, Left: SDS PAGE

			analysis of chromatography fractions; Right: purified hexamer (first 4 lanes) and monomer (last four lanes) uncleaved vs cleaved sample showing higher oligomeric states in hexamer sample shift upon cleavage of the C-terminal TwinStrep tag (uncropped gel images are shown in the Source Data). **c**, Sample micrograph of negatively stained *Dm*SERINC sample from 9.8-ml peak. **d**, 2D class averages of negatively stained *Dm*SERINC. **e**, Schematic of image processing and 3D reconstruction of the *Dm*SERINC hexamer. Volumes are shown at two contour levels, towards the protein level in solid white and the outline of the detergent micelle in transparent grey. Details of the image processing and reconstruction are given in Extended Methods. **f**, Left: Gold-standard FSC curve for the refined *Dm*SERINC cryo-EM map. **f**, Right: Euler angle distribution plot for aligned particles contributing to the 3D reconstruction; bar lengths and color (blue low, red high) correspond to numbers of particles in corresponding orientations. **g**, Cryo-EM map colored according to local resolution estimated with blocres and shown at high (left) and low (right) contour levels. **h**, Cryo-EM maps of the asymmetrical *Dm*SERINC hexamer (corresponding to 3D classes 3 and 8 in Extended Data Fig. 3e) with fitted model: viewed down 6-fold axis (top) or from side (bottom). The map is contoured to highlight the protein components (right) or the detergent micelle (left).
Extended Data Fig. 4	Structural features of DmSERINC	Extended_Data_Fig4_VEP.jpeg	**a**, Transmembrane topology diagram of *Dm*SERINC structure with residues not resolved in the cryo-EM map shaded grey. **b**,

			Topology diagram of the SERINC protein fold, colored as in Fig. 1b. ECLs and ICLs are labelled along with disulphide bonds and subdomains A and B. **c**, Scatter plot of top 500 results from analysis using Dali server, showing numbers of aligned residues versus root mean square deviations (Å) of Cα atom positions. **d**, *Dm*SERINC hexamer colored by conservation; Guillemet indicates the viewpoint on the protomer-protomer interface labeled with asterisk that is shown in the sideview on the right. **e**, Examples of *Dm*SERINC cryo-EM map with fitted model. **f**, Two disulphide bonds identified on the extracellular side of *Dm*SERINC. Left: Cryo-EM map showing profile of Cys71-Cys91 disulphide bond within ECL1. Right: Cryo-EM map showing profile of Cys238-Cys299 disulphide bond between ECL3 and ECL4. Thermostability of the *Dm*SERINC hexamer (**g**), monomer (**h**), and SERINC5 (**i**) with the addition of reducing agents (0.5 mM DTT and 0.5 mM TCEP); data shown are mean and s.d. n=3-4 technical repeats, data are provided in source data. **j,** Molecular dynamic simulations of solvation. Left top: Density analysis of waters (blue surface) around *Dm*SERINC (grey cartoon) in one repeat of atomistic 230-ns simulation. Left bottom: Water density shown as a 2D heatmap slice. Right: *Dm*SERINC residues implicated in controlling water wire highlighted in green.
Extended Data Fig. 5	Lipidomics of DmSERINC structure	Extended_Data_Fig5_VEP.jpeg	**a**, Cryo-EM map features of *Dm*SERINC displaying similarities with cardiolipin viewed with (right) and without (left) coordinates built, from two angles. **b**, Positions of the tentative cardiolipin sandwiched between the protomers of the hexamer. **c-e**, Identification of

			lipids associated with *Dm*SERINC by mass spectrometry: **c**, Lipidomics LC-MS analysis of hexameric *Dm*SERINC5 purified from yeast cells. Ions corresponding to phospholipids (PE, PC, PI) and cardiolipin compositions are indicated. **d**, Structures within each lipid class are confirmed by MS/MS fragmentation. Neutral loss fragments, such as R1COO- and R2COO- ions, are diagnostic for PE, PC, PI and cardiolipin (CL). **e**, Native mass spectra of *Dm*SERINC monomers (10^+ to 15^+ charge state distribution) isolated from LMNG micelles spiked with PC, PG, PE or CL lipids added at a 1:1 molar ratio. Up to two equivalents of bound CL were observed whereas no distinct binding was detected for PC, PG, or PE.
Extended Data Fig. 6	Lipid screening	Extended_Data_Fig6_VEP.jpeg	**a**, Lipid binding groove apparent in *Dm*SERINC structure, top left: Surface representation of *Dm*SERINC monomer revealing a groove formed between TMs 5, 7, 8 and 4. top right: Lipid moiety modeled into the groove, shown in spheres, illustrating complementary size, shape and location for lipid binding. bottom left: Cartoon representation of the same view with helices labelled and colored as Fig. 1b. bottom right: Cartoon representation with lipid shown in stick format. **b**, Cryo-EM map has lipid-like features in this groove, left: map with PS modelled in, right: map carved to 2.5 Å around the modelled PS to highlight the lipid-like map features. **e**. View of *Dm*SERINC in a POPC membrane, following 215 ns of atomistic simulation. The protein is shown as blue cartoon and transparent surface, and the POPC lipids as red, orange and grey spheres. Lipids in front of the protein have been removed to reveal how the protein sits in the

			membrane. **d**, Post 215 ns view of *Dm*SERINC from atomistic MD simulation, showing a POPC lipid bound to the groove between TM 5 and 8. The protein is shown in white cartoon, the lipid in green, red and gold spheres. Note that this lipid remains bound for the full simulation. **e-g**, Lipid thermostability assay. **e**, Change in thermostability of *Dm*SERINC hexamer upon the addition of specific lipid. **f**, Change in thermostability of *Dm*SERINC monomer upon the addition of a specific lipid; **g**, Change in thermostability of SERINC5 upon the addition of a specific lipid (select sample of lipids). Data shown in e-f are mean and s.d. of 3-6 technical repeats, data are provided in Source Data.
Extended Data Fig. 7	HDX of lipid interactions with DmSERINC	Extended_Data_Fig7_VEP.jpg	**a**, Left: Peptide coverage of *Dm*SERINC monomer for HDX. Right: Structure of *Dm*SERINC (with undefined loops modeled in using SWISS MODEL) with coverage highlighted in blue. **b-e**, HDX profile of purified monomeric *Dm*SERINC in LMNG micelles prior to (**b**) or after spiking with exogenous DPPS (**c**), sulfatides (**d**), or PC (**e**) Peptide residue numbers are shown on the x-axis. **f**, Protected regions determined by HDX mapped onto the *Dm*SERINC structure and highlighted in red (with undefined loops modelled in using SWISS MODEL). **g**, surface representation of *Dm*SERINC structure colored as in Fig. 1b. with protected regions highlighted in red.
Extended Data Fig. 8	Juxtaposition of SERINC5 and the trimeric HIV-1 envelope spike.	Extended_Data_Fig8_VEP.jpeg	The model of human SERINC5 is shown in grey cartoons with residues important for restriction highlighted in blue and modeled loops in white transparent. The illustrative model of full-length trimeric HIV-1 Env was assembled

			using PDB 6E8W (model 1; pinks) and PDB 5FUU (gp41 browns; gp120 purples), MPER (653-683) is shown in cyans, all structures shown in cartoons; membrane is in cream. **a**, Side-by-side comparison; **b**, Models shown in closer proximity, **c**, 90° rotation and zoom of model in panel b showing the distance between ECL5 and ECL3 is approximately the same distance (~30 Å) as that between MPER α helices in gp41.
Extended Data Fig. 9			
Extended Data Fig. 10			

1

Item	Present?	Filename This should be the name the file is saved as when it is uploaded to our system, and should include the file extension. The extension must be .pdf	A brief, numerical description of file contents. i.e.: *Supplementary Figures 1-4, Supplementary Discussion, and Supplementary Tables 1-4.*
Supplementary Information	Yes	Supplementary_all_together_VEP.pdf	Supplementary Tables 1-2 and Supplementary Note (Extended Methods).
Reporting Summary	Yes	Nr-reporting-summary1_VEP.pdf	

2

Type	Number If there are multiple files of the same type this should be the numerical indicator. i.e. "1" for Video 1, "2" for Video 2, etc.	Filename This should be the name the file is saved as when it is uploaded to our system, and should include the file extension. i.e.: *Smith_Supplementary_Video_1.mov*	Legend or Descriptive Caption Describe the contents of the file
Supplementary Video	1	Movie1_structure_of_DmSERINC.mov	Structure of DmSERINC
Supplementary Video	2	Movie2_structure_of_SERINC5	Structure of SERINC5

Choose an item.			
Choose an item.			
Choose an item.			
Choose an item.			

3

Figure	Filename This should be the name the file is saved as when it is uploaded to our system, and should include the file extension. i.e.: *Smith_SourceData_Fig1.xls*, or *Smith_ Unmodified_Gels_Fig1.pdf*	Data description i.e.: Unprocessed Western Blots and/or gels, Statistical Source Data, etc.
Source Data Fig. 1		
Source Data Fig. 2		
Source Data Fig. 3		
Source Data Fig. 4	SourceData_Figure4.xlsx source_data_blots_Fig4C .pdf	Statistical Source Data for Fig 4 a, b, e Unprocessed Western Blots for Fig 4c
Source Data Fig. 5		
Source Data Fig. 6		
Source Data Fig. 7		
Source Data Fig. 8		
Source Data Extended Data Fig. 1	source_data_blots_gels_ ExtData_Fig1a.pdf SourceData_ExtData_Fig 1.xlsx	Unprocessed Western Blots Statistical Source Data for Extended Data fig 1 c-e
Source Data Extended Data Fig. 2	source_data_gels_ExtDat a_2b.pdf	Unprocessed SDS PAGE gels
Source Data Extended Data Fig. 3	source_data_gels_ExtDat a_3b.pdf	Unprocessed SDS PAGE gels
Source Data Extended Data Fig. 4	ExtData_Fig4_thermosta bility_reducing_agents_s ource_data.xlsx	Statistical Source Data for Extended Data fig 4 g-i
Source Data Extended Data Fig. 5		

Source Data Extended Data Fig. 6	ExDataFig6_thermostability_lipids_source_data.xlsx	Statistical Source Data for Extended Data fig 6e-g
Source Data Extended Data Fig. 7		
Source Data Extended Data Fig. 8		
Source Data Extended Data Fig. 9		
Source Data Extended Data Fig. 10		

A bipartite structural organization defines the SERINC family of HIV-1 restriction factors

Valerie E. Pye[1], Annachiara Rosa[1&], Cinzia Bertelli[2&], Weston B. Struwe[3], Sarah L. Maslen[4], Robin Corey[5], Idlir Liko[3], Mark Hassall[6], Giada Mattiuzzo[6], Allison Ballandras-Colas[1], Andrea Nans[7], Yasuhiro Takeuchi[6,8], Phillip J. Stansfeld[5, 9], J. Mark Skehel[4], Carol V. Robinson[3], Massimo Pizzato[2*] & Peter Cherepanov[1,10*]

[1]Chromatin Structure and Mobile DNA Laboratory, Francis Crick Institute, 1 Midland Road, London, NW1 1AT, UK; [2]University of Trento, Department of Cellular, Computational and Integrative Biology, 38123 Povo, Italy; [3]Physical and Theoretical Chemistry Laboratory, South Parks Road, Oxford, OX1 3QZ, UK; [4]Biological Mass Spectrometry and Proteomics Laboratory, MRC Laboratory of Molecular Biology, Cambridge, CB2 0QH, UK; [5]Department of Biochemistry, University of Oxford, OX1 3QU, UK; [6]National Institute for Biological Standards and Control, Blanche Lane, South Mimms, Potters Bar, Hertfordshire, EN6 3QG, UK; [7]Structural Biology Science Technology Platform, Francis Crick Institute, NW1 1AT, UK; [8]UCL Division

of Infection and Immunity, The Rayne Building, 5 University Street, London, WC1E 6EJ, UK; [9]School of Life Sciences & Department of Chemistry, University of Warwick, Gibbet Hill Campus, CV4 7AL, UK; [10]Department of Medicine, Imperial College London, St-Mary's Campus, Norfolk Place, London, W2 1PG, UK.

[&]Contributed equally

*Correspondence:

Email: peter.cherepanov@crick.ac.uk (PC); massimo.pizzato@unitn.it (MP)

The human integral membrane protein SERINC5 potently restricts HIV-1 infectivity and sensitises the virus to antibody-mediated neutralisation. Here, using cryo-electron microscopy, we determined the structures of human SERINC5 and its ortholog from *Drosophila melanogaster* at sub-nm and near-atomic resolution, respectively. The structures reveal a novel fold comprised of ten transmembrane helices organised into two subdomains and bisected by a long diagonal helix. A lipid binding groove and clusters of conserved residues highlight potential functional sites. A structure-based mutagenesis scan identified surface-exposed regions and the interface between the subdomains of SERINC5 as critical for HIV-1 restriction activity. The same regions are also important for viral sensitisation to neutralising antibodies, directly linking the antiviral activity of SERINC5 with remodelling of the HIV-1 envelope glycoprotein.

Host organisms employ a range of mechanisms to impede replication of pathogens, and the latter evolve countermeasures to circumvent the innate immunity of their hosts[1]. One such antagonistic interaction involves the human transmembrane protein SERINC5, which when incorporated into budding HIV-1 virions, can strongly inhibit their subsequent entry into target cells[2,3]. To negate the effect of SERINC5, HIV-1 encodes the endocytic adaptor protein Nef, which redirects this restriction factor, normally present in the plasma membrane, to endosomal compartments, thereby preventing its inclusion into budding viral particles[2,3]. The ability to ablate plasma membrane-associated SERINC proteins is conserved among retroviruses[2-5], suggesting a strong evolutionary pressure to prevent virion incorporation of these host factors. Exclusive to eukaryotes, SERINCs share high amino acid identity among

themselves (Supplementary Table 1) but lack homology to any other known protein family. The term SERINC was coined after the proposed role of serine incorporation into membranes during lipid biosynthesis[6]. However, this function has so far not found independent confirmation, and mass spectrometry analyses failed to detect SERINC-dependent changes in cellular or virion lipid composition[7,8]. The human genome encodes five SERINC paralogs, of which one, SERINC2, lacks the HIV-1 restriction activity[9,10]. Recent studies highlighted associations of *SERINC* genes with autism[11], borderline personality disorders[12], alcohol dependence[13], and cancerogensis[14-17].

SERINC5 inhibits HIV-1 infectivity by specifically interfering with viral entry[2,3], although the precise mode of restriction remains enigmatic. HIV-1 particles assemble at lipid rafts within plasma membrane and utilize host endosomal sorting complexes required for transport (ESCRT) machinery to bud from the infected cell (reviewed in ref. 18). Following their maturation, virions infect target cells through fusion of the viral and host cell membranes. This process is orchestrated by the viral envelope glycoprotein (Env), which is a trimer comprised of the surface glycoprotein gp120 and the single-pass transmembrane subunit gp41, $(gp41\text{-}gp120)_3$. A series of conformational changes within HIV-1 Env, triggered by the interaction of gp120 with CD4 and a co-receptor (CCR5 or CXCR4) on surface of a target cell, lead to the insertion of the gp41 fusion peptide into the target cell plasma membrane. The subsequent collapse of the gp41 structure into a 6-helix bundle is believed to initiate the fusion of viral and host cell membranes[19]. HIV-1 Env is highly variable, and individual viral isolates display vastly different sensitivities to neutralizing antibodies and restriction by SERINC5. Thus, while SERINC5 can ablate infectivity of the HIV-1 clone NL4-3, it has only a modest effect on the tier 2 and 3 HIV-1 isolates,

such as JRFL[2,3,10,20,21]. Nevertheless, JRFL becomes considerably more sensitive to some neutralizing antibodies and the CCR5 antagonist Maraviroc in the presence of SERINC5, suggesting that the restriction factor exerts a direct effect on the conformation of HIV-1 Env[10,20].

Here we present the three-dimensional structure of a SERINC family member to near-atomic resolution and show that the observed conformation is consistent with that of human SERINC5, which we resolved at sub-nm resolution. Additionally, using an extensive panel of amino acid substitutions, we identify the regions of SERINC5 that are critical for its antiviral activities.

Results

Structure determination of *Drosophila melanogaster* SERINC. The fly possesses a single SERINC ortholog (referred to here as *Dm*SERINC, and also known as TMS1) that shares 36% amino acid sequence identity with human SERINC5 (Supplementary Table 1). Ectopic expression of *Dm*SERINC during production of Nef-deficient HIV-1 virions strongly suppressed their infectivity (Extended Data Fig. 1 a-c), confirming conservation of functional restriction by the insect ortholog. To structurally characterise the SERINC family of proteins, we produced recombinant human SERINC5 and *Dm*SERINC in human and yeast cells, respectively. When subjected to chromatography through a 24-ml Superdex-200 sizing column, SERINC5 migrated as a single peak with elution volume of 12 ml. Imaging negatively-stained material from this peak revealed featureless micelles, which failed to produce discrete 2D averages (Extended Data Fig. 2a-d). By contrast, separation of *Dm*SERINC resulted in an additional species eluting at 9.8 ml, containing well-defined assemblies with prominent six-fold symmetry (Extended Data Fig. 3a-d). Encouraged by these results,

we acquired micrograph movies of frozen-hydrated *Dm*SERINC from this fraction. Image processing of single particles resulted in a 3D reconstruction to an overall resolution of 3.3 Å with a local resolution of 2.8-3 Å for the majority of the protein (Extended Data Fig. 3e-g). Atomic coordinates were built *ab initio* into the cryo-EM map revealing the details of the homo-hexameric *Dm*SERINC structure (Fig. 1a,b, Table 1 and Supplementary Video 1).

Each of the six identical *Dm*SERINC subunits consists of ten transmembrane helices (TM) arranged into two subdomains revealing a tertiary fold that is ~35 Å by ~50 Å in the membrane plane and ~50 Å traversing the membrane (Fig. 1b). A 39-residue-long α-helix (TM4) spans the membrane diagonally intersecting subdomain A (TM1, TM2, TM3, TM9) and subdomain B (TM5, TM6, TM7 and TM10). A shorter diagonal α-helix TM8 crosses back from subdomain B to A, forming an asymmetrical cross with TM4 in the centre. Two disulphide bonds are identified on the extracellular side: one within extracellular loop (ECL) 1 (Cys71-Cys95, conserved in most species except plants and some lower eukaryotes) and one between ECL3 and ECL4 (Cys238-Cys299, conserved throughout the SERINC family) (Fig. 1b, Extended Data Fig. 4f, Supplementary Table 1 and Supplementary Video 1). Concordantly, exposure of *Dm*SERINC and SERINC5 to reducing agents decreased their thermostability (Extended Data Fig. 4g-i). The disulphide bonds and the location of ECL4, the equivalent of which harbours glycosylated Asn294 in SERINC5[22], confirms the assigned orientation within the plasma membrane, with both the N- and C-termini of the protein residing in the cytoplasm (Fig. 1b, Supplementary Table 1 and Extended Data Fig. 4a,b).

A query of the wwPDB using the Dali server[23] did not identify proteins sharing extensive structural similarity with *Dm*SERINC (Extended Data Fig. 4c).

Accordingly, the *Dm*SERINC structure represents a novel membrane protein fold. We considered if the hexameric arrangement of *Dm*SERINC was characteristic of the SERINC family. Protomer interface contacts bury 958 $Å^2$, comprising only 5.3% of the total *Dm*SERINC monomer surface. Furthermore, the interfaces are devoid of conserved amino acid residues (Extended Data Fig. 4d) and are largely lipid-mediated. Based on the cryo-EM map, we assigned one of the protomer-bridging lipids as cardiolipin and confirmed its presence in our *Dm*SERINC preparations by mass spectrometry (Extended Data Fig. 5). Consistent with the structure, we observed binding of up to two molecules of cardiolipin per *Dm*SERINC monomer (Extended Data Fig. 5e). We conclude that while the hexameric state of *Dm*SERINC made it conducive to high-resolution cryo-EM that afforded *de novo* model building, it may not be conserved throughout the protein family. Accordingly, we readdressed structural characterisation of human SERINC5 (see below).

Potential functional features of SERINC. Exploring the *Dm*SERINC structure further, we identified clusters of highly-conserved residues, which may represent functional sites in the fold (Fig. 2). Within subdomain A, lipid-buried Lys143 assembles with Tyr42, Gln136, Trp140, Tyr395, and His401 to form a small pocket at the membrane-cytosol interface (Fig. 2, bottom). At the extracellular side of the structure, Gln181, Tyr282, Tyr285, Ser289, Lys438, and Thr414 line a hydrophilic cleft between the two subdomains that is corked by Trp418. This crevice extends half-way through the lipid bilayer, where it is plugged by invariant Phe177 (Fig. 2, top). Molecular dynamics simulations of lipid-embedded *Dm*SERINC suggested that solvent molecules can freely enter the space between the subdomains (Extended Data

Fig. 4j). Searching structural databases with ProFunc[24] did not reveal similarity of either conserved pocket to any of the known functional sites.

The surface of subdomain B features an elongated groove formed by TM5, 7, 8 and the C-terminal end of TM4, which is an appropriate size, shape, and location to accommodate a lipid moiety, potentially allowing a head group to access the hydrophilic cleft between the subdomains (Extended Data Fig. 6a,b). When we embedded the protein structure in a lipid bilayer *in silico*, the groove became readily occupied by lipids during molecular dynamics (MD) simulations, and the cryo-EM map revealed presence of an acyl chain bound at this site (Extended Data Fig. 6c,d). We conducted a screen of lipids and found that addition of phosphatidylserine, cholesterol or sulfatide increased *Dm*SERINC and SERINC5 protein thermostability, while cardiolipin stabilised *Dm*SERINC only (Extended Data Fig. 6e-g). Moreover, hydrogen/deuterium exchange (HDX) experiments with *Dm*SERINC revealed that phosphatidylserine affected isotope exchange around the potential lipid binding groove in subdomain B (Extended Data Fig. 7).

The structure of human SERINC5. Composed of two subdomains, the *Dm*SERINC structure is suggestive of conformational flexibility. To determine if the conformation observed in *Dm*SERINC represents that of the *bona fide* HIV-1 restriction factor, we imaged SERINC5 in detergent micelles doped with phosphatidylserine, which was found to increase thermostability of the protein (Extended Data Fig. 6g). To aid in single particle image alignment of this 51 kDa protein, we acquired cryo-EM data in the presence of the antigen binding fragment (Fab) of a monoclonal antibody that recognizes SERINC5 ECL4. The resulting 3D reconstruction at a local resolution of 6.5-7 Å contains a single molecule of SERINC5 in a conformation very similar to that

of *Dm*SERINC protomers within the hexamer (Fig. 3, Extended Data Fig. 2 and Supplementary Video 2), leading us to conclude that the conformation we observe in the *Dm*SERINC structure is also adopted by human SERINC5.

Mapping SERINC5 regions critical for the antiviral activity. To identify regions of SERINC5 involved in HIV-1 restriction, we conducted an extensive mutagenesis screen, informed by the structure and amino acid sequence conservation with SERINC2, which lacks the HIV-1 restriction activity[9,10]. The mutations were introduced into constructs designed to express SERINC5 harbouring a FLAG epitope implanted within ECL4. This modification enabled surface exposure measurements of the modified proteins by flow cytometry without interfering with restriction activity (Extended Data Fig. 1d). In total, ninety-four SERINC5 mutants were tested for the ability to inhibit infectivity of Nef-negative HIV-1 (Fig. 4, Supplementary Table 2). The loss-of-function mutants clustered into two classes. The first class, comprising variants that also failed to localise to the plasma membrane, harboured the majority of mutants at highly conserved or invariant positions across the entire SERINC family, such as substitutions of Lys130, Phe165, Tyr388, His394, Trp411, Lys433, and Tyr444 (Fig. 4a). The second class of restriction-defective mutants retained the ability to localise to the plasma membrane. The majority of these carried substitutions within the ECLs or in proximity to the interface between the subdomains (Fig. 4b, d). This class included variants with substitutions within ECL5, such as a partial swap for the equivalent loop from SERINC2 (the mutant designated ECL5B), and double mutants NY413KP and IE419KM.

Next, we tested a representative subset of SERINC5 variants for incorporation into HIV-1 particles. As can be expected, class 1 mutants with severe defects in

surface expression (K130A and K433A) were deficient for glycosylation and failed to incorporate into virions (Fig. 4c), explaining their inability to restrict infection. In contrast, class 2 mutants that were competent for plasma membrane localization incorporated into viral particles (Fig. 4c). To test the ability of these mutants to remodel HIV-1 Env, we pseudotyped Nef-negative HIV-1 particles with the tier-2 glycoprotein JRFL, which is substantially resistant to restriction by SERINC5[3]. In agreement with published observations[10,20,25], the virus produced in the presence of WT SERINC5 displayed enhanced sensitivity to neutralisation by the monoclonal antibodies 4E10 and 2F5, both of which target the highly-conserved membrane external proximal region (MPER) of HIV-1 Env (Fig. 4e). Remarkably, class 2 SERINC5 mutants were substantially compromised in their ability to sensitize the virus to neutralization (Fig. 4e). Thus, despite incorporation into virions, class 2 mutants are defective for both of the antiviral activities.

Discussion

The conserved cellular functions of SERINCs remain unclear, underscoring the difficulty in determining structure-function relationships from first principles. Further studies will be required to test the functional significance of phosphatidylserine, sulfatide and/or cholesterol binding in biological functions of SERINC proteins. Affinity for cholesterol and/or exposed phosphatidylserine could help explain the association of SERINC5 with lipid rafts[9,26] and ultimately incorporation of the protein into budding virions.

The failure of class 1 SERINC5 mutants to inhibit HIV-1 infectivity strongly argues that the protein must be located at the plasma membrane to exert its antiviral activity. Intriguingly, despite virion incorporation, class 2 mutants were deficient for

both restriction and sensitization to neutralizing antibodies. The congruence of these antiviral activities suggests a specific interaction resulting in the conformational remodelling of surface-exposed regions of HIV-1 Env. The involvement of the ECLs and the interface between the subdomains in restriction suggests that the restriction depends on a specific conformation of SERINC5 and strongly indicates that this activity takes place on the external surface of the virion.

For illustrative purposes, we modelled the complete HIV-1 Env trimer using recent partial experimental structures[27,28] (Extended Data Fig. 8a). In contrast to the extended viral spike, SERINC5 is almost entirely membrane embedded, poised to reach only the membrane proximal and/or embedded regions of Env (Extended Data Fig. 8a). Intriguingly, the spacing between ECL3 and ECL5 of SERINC5, both of which are important for the antiviral activities, matches that between the MPER regions within the Env trimer (Extended Data Fig. 8b,c). We speculate that interaction with the neighbouring MPER domains could explain both the inhibition of HIV-1 fusion and the sensitization to 2F5 and 4E10 antibodies by SERINC5. This hypothesis is consistent with the genetic studies that mapped the determinants of SERINC5 sensitivity to the variable loops in gp120[20,29], as amino acid changes in the variable loops can modulate the accessibility of MPER[30]. Moreover, the interaction with CD4, which triggers an open HIV-1 Env conformation and increases MPER accessibility[31], rendered tier 2 and 3 viral isolates sensitive to restriction by SERINC5[21]. At present, we cannot exclude other possibilities, such as interactions with viral glycans and/or conformational movements of the spike that would enable direct SERINC5 contacts with gp120. Our structures and extensive functional data provide the initial insights at the molecular level of SERINC proteins and their ability to restrict HIV-1 infection,

warranting further research to clarify the molecular basis of the engagement between the host factor and HIV-1 Env.

Acknowledgements

We thank the UK Biological Services Division at the National Institute of Biological Standards and Control for their expertise in animal husbandry for the production of the antibody; R. Peat and the Cell Services Platform (Crick Institute) for upscaling of the hybridoma culture and purification of the antibody; J. Diffley for advice on codon-optimisation for protein expression in yeast; J. Frigola and G. Coster for the generous gift of JF1 cells and pGC014; R. Carzaniga for the maintenance of Vitrobot and Tecnai G2 microscope and user training; P. Walker, A. Purkiss and M. Oliveira for computer and software support; M. Silva dos Santos for assistance with lipid preparations; D. Wu (University of Oxford) for lipidomics support; the UK National Institute for Biological Standards and Control, and depositor H. Katinger, for providing anti-HIV-1 4E10, 2F5 and p55/p24 antibodies; A. Engelman (Dana-Farber Cancer Institute) and J. Luban (University of Massachusetts) for comments on the manuscript. PJS and RAC were funded by Wellcome Trust (208361/Z/17/Z). Research in PJS's lab is supported by the MRC (MR/S009213/1) and BBSRC (BB/P01948X/1, BB/R002517/1, BB/S003339/1). This project made use of time on ARCHER and JADE granted via the UK High-End Computing Consortium for Biomolecular Simulation, HECBioSim (http://hecbiosim.ac.uk), supported by EPSRC (grant no. EP/R029407/1). This research was funded by US National Institutes of Health grant P50 AI150481 and the Francis Crick Institute, which receives its core funding from Cancer Research UK (FC001061), the UK Medical Research Council (FC001061), and the Wellcome Trust (FC001061).

Author Contributions

V.E.P. expressed, purified and characterised *Dm*SERINC, built the atomic model, developed and conducted thermostability assays; V.E.P., P.C., and A.B.-C. prepared and screened cryo-EM grids; A.N. collected all cryo-EM data; V.E.P. and P.C. refined the *Dm*SERINC structure; A.R. and P.C. generated stable cell line for SERINC5 expression, purified and characterised SERINC5 and determined the structure; A.R. conducted thermostability assays on SERINC5 and purified the Fab; P.C. produced mutant SERINC5 constructs; M.P. and C.B. developed and performed assays to measure surface exposure, restriction activity and virion incorporation of SERINC5 variants; W.B.S., I.L. and C.V.R. analysed lipid composition of *Dm*SERINC preparations; S.L.M. and J.M.S. designed, conducted and analysed HDX/MS experiments; R.C. and P.S. conducted MD simulations on lipid-imbedded *Dm*SERINC; M.H., G.M. and Y.T. generated hybridomas for monoclonal anti-SERINC5 antibody; P.C. and M.P. conceived and directed the work; V.E.P., M.P. and P.C. wrote the manuscript with contributions from all authors.

Ethics declarations

Competing interests

The authors declare no competing interests.

Figure Legends

Figure 1 | The structure of *Dm*SERINC. a, Cryo-EM map of the hexamer with each protomer individually colored; the map was Gaussian filtered with a standard deviation of 5 Å to represent the detergent micelle, grey (left) and a cartoon representation of the *Dm*SERINC hexamer (right). **b**, Detailed representation of an isolated monomer, colored in green to dark blue gradient from N- to C-terminus with transmembrane alpha helices numbered and loops labelled (intracellular loops (ICL) and extracellular loops (ECL)). The position of the lipid groove is indicated by a grey rectangle. Disulphide bonds are labelled and shown in stick format. The outer and inner plasma membrane surfaces are depicted as chocolate and olive dotted planes, respectively.

Figure 2 | Potential functional sites identified in SERINC structure. Sequence conservation mapped onto the *Dm*SERINC structure, with invariant residues in dark blue and most variable in red; the outer and inner plasma membrane surfaces are depicted as chocolate and olive dotted planes, respectively. The insets show details of the hydrophilic cleft between the subdomains (top) and a highly conserved pocket (bottom).

Figure 3 | Structure of human SERINC5 bound to Fab. The cryo-EM map is shown as a semi-transparent white surface, with fitted atomic models of *Dm*SERINC (cartoons colored as in Fig. 1b) and Fab (purple cartoons). Top view shows transmembrane helices traversing the detergent micelle and bottom view is a perpendicular slice showing SERINC5 surrounded by the micelle.

Figure 4 | SERINC5 residues critical for HIV-1 restriction activity. a and **b,** restriction activity and surface expression of human SERINC5 variants relative to SERINC5 wt (data shown are mean and s.d. of n=3 independent experiments). **a**, Class 1 amino acid substitutions interfere with Nef-defective HIV-1_{NL4-3} restriction and surface expression. **b**, Class 2 amino acid substitutions do not affect surface expression but compromise Nef-defective HIV-1 restriction. **c**, SERINC5 incorporation into virion particles. Immunoblots of Nef-defective HIV-1 particles and corresponding producer cell lysates expressing the indicated SERINC5 variants. The right-most lane contains a Gag-defective provirus control. Arrowheads and asterisks indicate migration position of glycosylated and non-glycosylated SERINC5, respectively. Note the selective incorporation of the glycosylated form into viral particles[22] **d**, Class 1 and 2 residues mapped onto a model of SERINC5, in red and blue, respectively. **e**, Neutralisation of Nef-deficient HIV-1_{NL4-3} carrying the JRFL envelope by 2F5 and 4E10 monoclonal antibodies. Residual infectivity is relative to that of untreated viruses (n=4, mean ± 95% confidence interval, technical repeats), IC_{50} values are shown in Extended Data Fig. 1e. Uncropped images for panel c and data for graphs a, b and e are available as Source Data.

Table 1. **Cryo-EM data collection, refinement and validation statistics**

	***Dm*SERINC** (EMD-10279, PDB 6SP2)	**SERINC5** (EMD-10277)
Data collection and processing		
Magnification	36,232	128,440
Voltage (kV)	300	300
Electron exposure ($e^-/Å^2$)	50	33.6
Defocus range (μm)	-1.6 to -4	-1.6 to -4
Pixel size (Å)	1.38	1.09
Symmetry imposed	C6	C1
Initial particle images (no.)	1,857,080	2,502,546
Final particle images (no.)	159,252	270,151
Map resolution (Å)	3.3	7.1
FSC threshold	0.143	0.143
Map resolution range (Å)	2.8-50.0	6.5-50
Refinement		
Model resolution (Å)	3.3	
FSC threshold	0.143	
Model resolution range (Å)	2.8-4.0	
Map sharpening *B* factor ($Å^2$)	-186.2	
Model composition		
Nonhydrogen atoms	18,498	
Protein residues	2,190	
Ligands	CDL:6, LMN:12, P5S:6	
B factors ($Å^2$)		
Protein	150.59	
Ligand	163.13	
R.m.s. deviations		
Bond lengths (Å)	0.004	
Bond angles (°)	0.72	
Validation		
MolProbity score	1.77	
Clashscore	8.22	
Poor rotamers (%)	0.0	
Ramachandran plot		
Favored (%)	95.28	
Allowed (%)	4.72	
Disallowed (%)	0	

References

1. Duggal, N.K. & Emerman, M. Evolutionary conflicts between viruses and restriction factors shape immunity. *Nat Rev Immunol* **12**, 687-95 (2012).
2. Rosa, A. et al. HIV-1 Nef promotes infection by excluding SERINC5 from virion incorporation. *Nature* **526**, 212-7 (2015).
3. Usami, Y., Wu, Y. & Gottlinger, H.G. SERINC3 and SERINC5 restrict HIV-1 infectivity and are counteracted by Nef. *Nature* **526**, 218-23 (2015).
4. Chande, A. et al. S2 from equine infectious anemia virus is an infectivity factor which counteracts the retroviral inhibitors SERINC5 and SERINC3. *Proc Natl Acad Sci U S A* **113**, 13197-13202 (2016).
5. Ahmad, I. et al. The retroviral accessory proteins S2, Nef, and glycoMA use similar mechanisms for antagonizing the host restriction factor SERINC5. *J Biol Chem* **294**, 7013-7024 (2019).
6. Inuzuka, M., Hayakawa, M. & Ingi, T. Serinc, an activity-regulated protein family, incorporates serine into membrane lipid synthesis. *J Biol Chem* **280**, 35776-83 (2005).
7. Trautz, B. et al. The host-cell restriction factor SERINC5 restricts HIV-1 infectivity without altering the lipid composition and organization of viral particles. *J Biol Chem* **292**, 13702-13713 (2017).
8. Chu, E.P. et al. Disruption of Serinc1, which facilitates serine-derived lipid synthesis, fails to alter macrophage function, lymphocyte proliferation or autoimmune disease susceptibility. *Mol Immunol* **82**, 19-33 (2017).
9. Schulte, B. et al. Localization to detergent-resistant membranes and HIV-1 core entry inhibition correlate with HIV-1 restriction by SERINC5. *Virology* **515**, 52-65 (2018).

10. Sood, C., Marin, M., Chande, A., Pizzato, M. & Melikyan, G.B. SERINC5 protein inhibits HIV-1 fusion pore formation by promoting functional inactivation of envelope glycoproteins. *J Biol Chem* **292**, 6014-6026 (2017).

11. Hnoonual, A. et al. Chromosomal microarray analysis in a cohort of underrepresented population identifies SERINC2 as a novel candidate gene for autism spectrum disorder. *Sci Rep* **7**, 12096 (2017).

12. Lubke, G.H. et al. Genome-wide analyses of borderline personality features. *Mol Psychiatry* **19**, 923-9 (2014).

13. Zuo, L. et al. Rare SERINC2 variants are specific for alcohol dependence in individuals of European descent. *Pharmacogenet Genomics* **23**, 395-402 (2013).

14. Zeng, Y. et al. SERINC2-knockdown inhibits proliferation, migration and invasion in lung adenocarcinoma. *Oncol Lett* **16**, 5916-5922 (2018).

15. Bossolasco, M., Veillette, F., Bertrand, R. & Mes-Masson, A.M. Human TDE1, a TDE1/TMS family member, inhibits apoptosis in vitro and stimulates in vivo tumorigenesis. *Oncogene* **25**, 4549-58 (2006).

16. Margue, C. et al. New target genes of MITF-induced microRNA-211 contribute to melanoma cell invasion. *PLoS One* **8**, e73473 (2013).

17. Player, A. et al. Identification of TDE2 gene and its expression in non-small cell lung cancer. *Int J Cancer* **107**, 238-43 (2003).

18. Hurley, J.H. & Cada, A.K. Inside job: how the ESCRTs release HIV-1 from infected cells. *Biochem Soc Trans* **46**, 1029-1036 (2018).

19. Chen, B. Molecular Mechanism of HIV-1 Entry. *Trends Microbiol* **27**, 878-891 (2019).

20. Beitari, S., Ding, S., Pan, Q., Finzi, A. & Liang, C. Effect of HIV-1 Env on SERINC5 Antagonism. *J Virol* **91**(2017).

21. Zhang, X. et al. CD4 expression and Env conformation are critical for HIV-1 restriction by SERINC5. *J Virol* (2019).

22. Sharma, S., Lewinski, M.K. & Guatelli, J. An N-Glycosylated Form of SERINC5 Is Specifically Incorporated into HIV-1 Virions. *J Virol* **92**(2018).

23. Holm, L. & Sander, C. Dali: a network tool for protein structure comparison. *Trends Biochem Sci* **20**, 478-80 (1995).

24. Laskowski, R.A. The ProFunc Function Prediction Server. *Methods Mol Biol* **1611**, 75-95 (2017).

25. Lai, R.P. et al. Nef decreases HIV-1 sensitivity to neutralizing antibodies that target the membrane-proximal external region of TMgp41. *PLoS Pathog* **7**, e1002442 (2011).

26. Brugger, B. et al. The HIV lipidome: a raft with an unusual composition. *Proc Natl Acad Sci U S A* **103**, 2641-6 (2006).

27. Fu, Q. et al. Structure of the membrane proximal external region of HIV-1 envelope glycoprotein. *Proc Natl Acad Sci U S A* **115**, E8892-E8899 (2018).

28. Lee, J.H., Ozorowski, G. & Ward, A.B. Cryo-EM structure of a native, fully glycosylated, cleaved HIV-1 envelope trimer. *Science* **351**, 1043-8 (2016).

29. Usami, Y. & Gottlinger, H. HIV-1 Nef responsiveness is determined by Env variable regions involved in trimer association and correlates with neutralization sensitivity. *Cell Rep* **5**, 802-12 (2013).

30. Chakrabarti, B.K. et al. Direct antibody access to the HIV-1 membrane-proximal external region positively correlates with neutralization sensitivity. *J Virol* **85**, 8217-26 (2011).

31. Ivan, B., Sun, Z., Subbaraman, H., Friedrich, N. & Trkola, A. CD4 occupancy triggers sequential pre-fusion conformational states of the HIV-1 envelope trimer with relevance for broadly neutralizing antibody activity. *PLoS Biol* **17**, e3000114 (2019).

Methods

Protein expression and purification. *Dm*SERINC carrying a C-terminal TwinStrep tag was over-expressed in *S. cerevisiae* and solubilised in a buffer containing 1.5% n-dodecyl-β-D-maltoside (DDM, Anatrace). During affinity purification the detergent was exchanged to 0.05% lauryl maltose neopentyl glycol (LMNG, Anatrace), the concentration of which was reduced to a minimum for size exclusion chromatography. Human SERINC5 protein was purified from a stable cell line adapted to suspension culture following the protocol for *Dm*SERINC with the addition of 1,2-dipalmitoyl-*sn*-glycero-3-phosphoserine (DPPS; Echelon Biosciences) in the sample for cryo-EM. Detailed descriptions are in Supplementary Note 1.

Generation of the monoclonal antibody and the Fab to SERINC5. A monoclonal antibody EVG_S5.2 was produced in a single mouse immunised with recombinant SERINC5. A hybridoma line producing the antibody was expanded, and the Fab fragment was produced by digestion of the antibody with papain. Detailed descriptions are in Supplementary Note 1, and the monoclonal antibody is available from the Centre for AIDS Reagents (CFAR, www.NIBSC.org) for distribution.

Negative-stain EM. Purified *Dm*SERINC and SERINC5 (4 µl of ~0.01 mg/ml) were applied to glow-discharged carbon-coated 300-mesh copper grids (EM Resolutions) for 1 min before brief blotting and staining with 2 % (w/v) uranyl acetate. Grids were imaged on a Tecnai G2 Spirit LaB6 transmission electron microscope (FEI) operating at 120 keV. Images were collected with an Ultrascan-1000 camera (Gatan) at a nominal magnification of 30,000× (corresponding to a pixel size of 3.45 Å at the specimen level), with an average electron dose of 35 e/Å^2 and defocus values of -0.5 to -2.0 µm. Particles, picked semi-automatically using EMAN2 Boxer tool[32], were subjected to reference-free 2D classification in Relion-2.03[33] or cryoSPARC[34].

Cryo-EM grid preparation and data collection. Four µl of hexameric *Dm*SERINC at 0.5 mg/ml, freshly isolated by size exclusion chromatography, was applied onto glow-discharged holey carbon 400-mesh Quantifoil R1.2/1.3 grids (Quantifoil) for 1 min, with 100% humidity at 20°C, before blotting for 3-4 sec and plunge freezing into liquid ethane using Vitrobot Mark IV (FEI). Data were collected on a Titan Krios microscope operating at 300 keV and equipped with a Gatan post-column energy filter, selecting a 20-eV window, on a GIF Quantum K2 direct electron detector (Gatan) operating in counting mode. A total of 5,807 movies were recorded using single electron counting mode with a magnified pixel size of 1.38 Å and a defocus range of -1.6 to -4 µm. The total electron dose was 50 e^-/Å^2, spread over 30 frames (Table 1).

Freshly isolated SERINC5 in LMNG micelles supplemented with DPPS and equimolar amount of Fab was subjected to size exclusion chromatography through a Superdex 200 Increase 3.2/300 column. Four µl of isolated SERINC5-Fab complex

was applied onto non-glow discharged C-flat 400-mesh R1.2/1.3 holey carbon grids (EMS) for 30 sec under 100% humidity at 20°C, blotted for 7 sec, and vitrified by plunging into liquid ethane using Vitrobot Mark IV. Data were collected on a Titan Krios microscope at 300 keV equipped with a Falcon 3 detector. A total 7,165 movies were recorded in single electron counting mode with a pixel size of 1.09 Å and a defocus range -1.6 to -4 μm, using total electron doze of 33.6 e^{-}/Å^{2} over 30 frames (Table 1).

Cryo-EM image processing and 3D reconstruction. Micrograph movies were aligned with dose weighting applied as implemented in MotionCor2[35] and the contrast transfer function (CTF) parameters were estimated from the frame sums using Gctf-v1.06[36]. Movies exhibiting ice contamination were discarded at this stage, leaving 4,238 (*Dm*SERINC) and 7,021 (SERINC5-Fab complex) movies for further processing. A sub-set of particles semi-automatically picked in EMAN2 Boxer[32] were used to generate the starting 2D class averages, which, upon low-pass filtering to 20 Å, served as templates for auto-picking of the entire dataset (Extended Data Fig. 3e).

The initial *Dm*SERINC particle dataset was picked with Relion-2.1[33] resulting in 1,857,080 particles. Reference-free 2D classification was performed in cryoSPARC using 40 online-EM iterations into 200 classes. Particles belonging to well-defined 2D classes exhibiting secondary structure elements (717,011 particles) were selected for further processing. The starting model for 3D classifications was obtained using *ab initio* mode of cryoSPARC. 3D classification was carried out using Relion-2.1 into 9 classes without applying symmetry; the hexamer class (159,252 particles) was *in silico* purified from other states. The final 3D reconstruction was obtained using non-uniform refinement as implemented in cryoSPARC2 with C6 symmetry applied.

Classes containing asymmetrical hexamers (classes 3 and 8; Extended Data Fig. 3e) were investigated further, implementing C1 symmetry, to determine any structural rearrangements compared with the hexamer. The asymmetrical hexamers exhibited the exact same secondary structure conformations as the hexamer however were lacking some of the detergent micelle on one side (Extended Data Fig. 3h). Dimers of hexamers were also present in the sample (classes 1, 2, 4, 7 and 9; Extended Data Fig. 3e) and were likely formed by asymmetrical hexamers as a consequence of the limiting concentration of detergent used in sample preparation.

2,502,546 particles of SERINC5-Fab complex, autopicked using Gautomatch (http://www.mrc-lmb.cam.ac.uk/kzhang/), were subjected to reference-free 2D classification in cryoSPARC. The initial 3D model was obtained using *ab initio* reconstruction in cryoSPARC from a subset of particles belonging to 2D classes displaying clear density attributable to Fab. A total of 1,449,789 particles from well-defined 2D classes were subjected to classification in Relion-3 into eleven 3D classes. The most populated class containing 270,151 particles displayed high-resolution features with strong density corresponding to Fab outside and SERINC5 TMs inside the micelle. These particles were used for 3D auto-refinement in Relion-3 with a soft mask around the entire particle using C1 symmetry, including the detergent micelle resulting in a 3D reconstruction to an overall resolution of 8.2 Å and a local resolution throughout the protein density of 6.5-7 Å (Extended Data Fig. 2e-g). Resolution is reported according to the gold-standard Fourier shell correlation (FSC), using the 0.143 criterion[37] (Table 1, Extended Data Figs 2f,g and 3f,g). Local resolution was estimated using blocres tool from BSOFT package [38].

Model building and refinement. The *Dm*SERINC model was built *ab initio* into the cryo-EM map using Coot[39]. Initially, poly-Ala α-helices were placed for each of the 10 TM regions in one monomer and bulky side-chain features for aromatic residues were used to identify the sequence register. Further residues were added manually to complete one subunit of the hexameric ring, this was then used to generate the remaining five monomers in the hexamer. The hexameric model was then subjected to real space refinement using Phenix[40,41] with NCS constraints and refining group B-factors (one per residue) and assessed using MolProbity[42] and EMringer[43]. The final model contains 365 amino acid residues per subunit, lacking N-terminal peptide (residues 1-29) and portions of ECL1 (residues 75-89), ECL4 (residues 306-321), ICL4 (residues 354-389), and the C-terminal peptide (residues 462-465) as illustrated in the topology diagram in Extended Data Fig. 4a. One cardiolipin, two LMNG, and one PS molecule per monomer were tentatively built into the cryo-EM map and are included in the co-ordinates. Data statistics are given in Table 1. A homology model of SERINC5 was assembled based on *Dm*SERINC structure using SWISS-MODEL server[44]. Interface surface areas were calculated using the PISA server[45], and membrane buried regions were predicted using the PPM server[46].

Molecular dynamics. The atomic coordinates of *Dm*SERINC (protein only) were converted to their Martini CG representation[47,48], and built into POPC membranes. Missing loops were modelled using SWISS-MODEL[44], with the loop between TM1 and TM2 modelled as $(GlySer)_3$ hexapeptide, the loop between TM7 and TM8 modelled using the native structure (MFGMMEG), and the loop between TM8 and TM9 modelled as $(GlySer)_7$. Simulations were run over 100 ns using a 20 fs time-

step, in the NPT ensemble at 323 K with the V-rescale thermostat, and 1 bar using semi-isotropic Berendsen pressure coupling.

Atomistic simulations were run following conversion of 100 ns CGMD snapshots in a POPC bilayer. Conversions were carried out using the CG2AT protocol[49], with Charmm36 forcefield[50] used to describe the system. Electrostatics were handled using the Particle-Mesh-Ewald method, and a force-switch modifier was applied to the Van der Waals forces. Dispersion corrections were turned off. Simulations were run for ~215 ns with Velocity-rescaling temperature coupling at 310 K using a time constant of 0.1 ps and Parrinello-Rahman semi-isotropic pressure coupling of 1 Bar with a time constant of 2 ps, using 4 fs time steps with virtual-sites on the protein and lipids[51]. All simulations were run in Gromacs 2018[52]; images were made in VMD[53].

Infectivity assays. The effect of SERINC5 mutants on the infectivity of HIV-1 was studied using virions limited to a single round of replication. To this end, 200,000 HEK293T cells were transfected with 800 ng of an *env*-defective and *nef*-defective HIV-1_{NL4-3} provirus construct together with 100 ng of PBJ5-HXB2-Env[2] and a plasmid encoding variants of SERINC5 harbouring an internal FLAG epitope (DYKDDDDKDI, inserted between residues 290 and 291) and a C-terminal HA tag (SERINC5-iFLAG, HA), or an appropriate empty vector control using calcium phosphate. High-level overexpression of SERINC5 results in suppression of viral release, which is not characteristic of the restriction factor at endogenous levels[2]. Therefore, SERINC5 mutants were tested using constructs based on pBJ6 or pBJ5, both of which harbour a weak promoter, resulting in moderate and low expression compared to pcDNA, respectively[2]. All experiments used a matched wild type

583 SERINC5 control and the constructs and amount of SERINC5 expressing plasmid
584 used in specific experiments are described in Supplementary Table 2. Virus-
585 containing culture supernatants were collected 48 h after transfection, clarified by
586 centrifugation at 300*g* for 5 min and passed through a 0.45-µm filter. Virus in cell
587 supernatants was quantified using the Sybr Green PCR-enhanced reverse transcriptase
588 assay[25,54], and five serial dilutions were inoculated onto HeLa-TZM-GFP reporter
589 cells, which contain an integrated reporter gene encoding GFP with a nuclear
590 localization signal under the transcriptional control of the HIV-1 long terminal
591 repeat[2]. Infections were performed in quadruplicate and the number of cells infected
592 was evaluated using an EnSight plate reader (Perkin Elmer). Infectivity was measured
593 by normalizing numbers of infected cells according to the reverse transcriptase
594 activity in each viral preparation. Only dilutions within a linear range were
595 considered. Reduction of infectivity caused by SERINC5 proteins was then calculated
596 by dividing the infectivity of viruses produced in the absence of SERINC5 with the
597 infectivity of viruses produced when co-expressing SERINC5. The residual restriction
598 activity of each SERINC5 mutant on HIV-1 infectivity was then expressed in relation
599 to the reduction caused by the wild type protein, considered as 100%. Where error
600 bars are present, they represent standard error of the mean obtained from three
601 independent biological triplicates or four technical replicates as indicated.
602
603 **Surface exposure of SERINC5 mutants.** To investigate SERINC5 expression by
604 flow cytometry, 200,000 HEK293T cells were co-transfected with DNA constructs
605 expressing SERINC5-iFLAG-HA variants based on either pcDNA3.1 or pBJ5 vectors
606 as indicated in Supplementary Table 2 along with 300 ng pIRES2-GFP, to allow for
607 selective gating of transfected cells, and 1 µg pBluescript. Forty-eight h post-

transfection, cells were collected, washed with ice-cold PBS and fixed with 2% paraformaldehyde. Each sample was then divided in two, and processed for staining with anti-FLAG antibody for selective detection of SERINC5 on the cell surface in non-permeabilized cells or for detection of total SERINC5 expression after permeabilisation with Wash&Perm solution (Becton Dickinson). SERINC5-iFLAG-HA was detected using mouse M2 anti-FLAG antibody (Sigma) diluted 1:500 and an APC-conjugated anti-mouse IgG (Jackson Immunoresearch) diluted 1:500. Samples were analysed using a FACS Canto (Becton Dickinson). SERINC5 expression was assessed on the live cell population gated on FSC vs SSC, followed by gating the transfected cell population, which express GFP, as illustrated in Supplementary Information Table 2.

SERINC5 incorporation into virus particles and immunoblotting. To detect SERINC5 associated with virus particles, 5 million HEK293T cells were transfected with 18 µg *env*-defective and *nef*-defective HIV-1_{NL4-3} provirus construct together with 2 µg pBJ5-HXB2-Env and 1 µg pBJ5-SERINC5-iFLAG-HA. To verify specific detection of virus-associated SERINC5, a control sample was produced by transfecting a Gag-defective HIV-1_{NL4-3} provirus construct. Cell supernatants from transfected cells were clarified by centrifugation at 300*g* for 5 min, passed through filters with 0.45-µm pores, overlaid on a 25% sucrose cushion and concentrated by centrifugation for 2 h at 100,000*g* in a SW41 swingout rotor (Beckman Coulter). The resulting viral pellets were resuspended in Laemmli sample buffer supplemented with 50 mM TCEP. Virus producing cells were collected in PBS, pelleted and lysed in an ice-cold buffer containing 100 mM NaCl, 10 mM HEPES pH 7.5, 1% DDM and protease inhibitors. Lysates, clarified by centrifugation and mixed with Laemmli

633 buffer supplemented with 50 mM TCEP, were separated on 12.5% acrylamide Tricine
634 gels and transferred onto Immobilon-FL PVDF membrane (Millipore). Blots were
635 probed with mouse anti-HA (clone 16B12, Covance) diluted 1:1,000, rabbit anti-
636 β actin (Li-COR) diluted 1:1,000 and rabbit anti-HIV-1 p24 (ARP432; National
637 Institute for Biological Standards and Control) antibody. Secondary antibodies were
638 conjugated to IRDye 680 or IRDye 800 (Li-COR), and blots were imaged using an
639 Odyssey infrared imaging System (Li-COR).
640
641 **HIV-1 neutralization assays.** Sensitivity to neutralizing antibodies was measured
642 using virions limited to a single round of replication produced by transfection of
643 HEK293T cells similarly to as described for the infectivity assay, with the only
644 difference that the HIV-1_{NL4-3} Env defective provirus construct was complemented in
645 *trans* with a vector encoding Env derived from HIV-1_{JRFL} (pSV-JRFL), which allows
646 production of virions minimally sensitive to the effect of SERINC5 on infectivity.
647 Viruses were normalized based on reverse transcriptase activity and the inocula were
648 adjusted to produce between 1% and 3% infection of the monolayer. Viruses were
649 incubated with serially diluted neutralizing antibodies for 1 h at room temperature.
650 The complexes were added to TZM-bl GFP cells, seeded onto 96-well tissue culture
651 plates a day prior to neutralization, incubated at 37°C for 2 h, followed by two washes
652 with PBS before being cultured in fresh complete DMEM. Infected cells were
653 incubated at 37°C for 42 h before scoring number of infected cells per each well using
654 an Ensight plate reader.
655 Neutralization was measured by calculating the residual infectivity of treated
656 virus samples considering the infectivity of the untreated sample as 100%. Fitted
657 sigmoidal curves and the IC_{50} values were obtained using Prism (Graphpad) with the

least square variable slope method using the dose-normalized response protocol. Neutralizations were performed in quadruplicate with each combination of virus and antibody to be analyzed and data shown are the average with the error bars representing the 95% confidence interval as calculated by Prism. Neutralizing antibodies 4E10 (ARP3239) and 2F5 (ARP3063) were obtained from the UK National Institute for Biological Standards and Control.

Protein thermostability assay. Melting curves were recorded using 20-95°C 1.5°C/min temperature ramps on a Promethius NT.48 instrument with standard capillaries (Nanotemper). Proteins were diluted to 1 mg/ml in 40 mM NaCl, 10 mM HEPES-NaOH, pH 7.5, 0.0003% LMNG; where indicated, samples were spiked with 0.1 mM lipid. Lipid stock details are given in Supplementary Note 1.

Native protein mass spectrometry. Purified *Dm*SERINC was buffer exchanged into 200 mM ammonium acetate, pH7 supplemented with 0.002% LMNG using Bio-Spin 6 Columns (BioRad). Samples were analysed at a final concentration of 5 μM using a Q-Exactive mass spectrometer (Thermo Fisher Scientific) modified for high molecular weight ions as previously described[55]. Cardiolipin (Avanti), PI(3,4)P2 (Avanti), PI(4,5)P2 (Avanti), POPE (Avanti), POPC (Avanti) and POPG (Avanti) were reconstituted to 3 mM in 200 mM ammonium acetate supplemented with 0.017% DDM and diluted into the desired concentration using 200 mM ammonium acetate with 0.002% LMNG. Lipids were added to *Dm*SERINC samples and equilibrated for 20 min prior to analysis. Ions were generated by static nano-electrospray using gold-coated capillaries prepared in-house as described previously[56]. Instrument settings were as follows: capillary voltage 1.5 kV, source

temperature 40°C, S-lens RF = 200, maximum injection time 150, HCD voltage 200 V, desolvation voltage -10 (positive mode), with in-source trapping on. Data were acquired between 2,000-15,000 with 10 microscans, and results were processed using XCalibur 2.2 software (Thermo Fisher Scientific). *Dm*SERINC peak assignments were done manually using in-house software as well as with UniDec software[57].

Lipidomics. Sequencing grade trypsin (Promega) was added to 20 µg *Dm*SERINC (5:1 SERINC to trypsin) and incubated overnight at 37°C. Samples were dried in a vacuum concentrator and reconstituted (15 min sonication) in 30 µl acetonitrile:water (60:40, v/v), 10 mM ammonium formate, 0.1% formic acid (buffer A). Samples were centrifuged for 3 min at 10,000*g* and 15 µl was removed for analysis. For each run, 5 µl was injected onto a C18 column (Acclaim PepMap 100, C18, 75 mm × 15 cm; Thermo Scientific) on a Dionex UltiMate 3000 RSLC nanoLC System. A 32-99% linear gradient to buffer B (isopropanol:acetonitrile (90:10, v/v), 10 mM ammonium formate, 0.1% formic acid) was used with a flow rate of 300 nl/min over 30 min. Data were acquired using an LTQ Orbitrap mass spectrometer (Thermo Fisher Scientific) in negative ion mode with the following data-dependent acquisition settings: full-scan mass range 350-2,000 *m/z*, resolution 60,000, normalized collision energy 38%, activation time 30 msec, automatic gain control target 30,000, capillary voltage 1.8 kV, and capillary temperature 180°C. Collision-induced dissociation was performed for the five most intense ions, data were interpreted manually using XCalibur 2.2 software (ThermoFisher Scientific).

HDX mass spectrometry. Deuterium exchange reactions of *Dm*SERINC (monomeric fraction) in LMNG micelles with or without addition of exogenous DPPS

(Echelon Biosciences), sulfatide (Matreya LLC) or PC (Echelon Biosciences), were initiated by diluting the proteins in D_2O (99.8% D_2O, Sigma-Aldrich) in 10 mM HEPES pH 7.5, 40 mM NaCl, 2 mM DTT and 1 mM TCEP to obtain a final D2O concentration of ~91%. For all experiments, deuterium labelling was carried out at 23°C (unless otherwise stated) at four points, 3, 30, 300, and 3,000 sec in triplicate. The exchange was quenched by the addition of chilled 2 M guanidinium hydrochloride in 100 mM phosphate buffer, pH 2.4 (adjusted with formic acid), 15 mM TCEP and 0.1% v/v DDM. Samples, snap frozen in liquid nitrogen, were stored at -80°C prior to analysis.

The quenched protein samples were rapidly thawed and subjected to proteolytic cleavage with pepsin followed by reversed phase chromatography. Briefly, the protein was passed through a 5-μm 2.1 × 30 mm Enzymate BEH immobilized pepsin column, (Waters) at 200 μl/min for 2 min; the peptic fragments were trapped and desalted on a 1.7-μm 2.1 × 5 mm C18 trap column equipped with Acquity BEH C18 Van-guard pre-column (Waters). Trapped peptides were subsequently eluted over 11 min with a 3%–43% gradient of acetonitrile in 0.1% v/v formic acid at 40 μl/min. Peptides were separated on a reverse phase column (Acquity UPLC BEH C18 column 1.7 μm, 100 mm x 1 mm, Waters) and detected on a SYNAPT G2-Si HDMS mass spectrometer (Waters) over a *m/z* of 300 to 2000, with the standard electrospray ionization (ESI) source with lock mass calibration using [Glu1]-fibrino peptide B (50 fmol/μl). The mass spectrometer was operated at a source temperature of 80°C and a spray voltage of 2.6 kV. Spectra were collected in positive ion mode. Peptide identification was performed by MS^{E58} using an identical gradient of increasing acetonitrile in 0.1% v/v formic acid over 11 min.

The resulting MS data were analysed using Protein Lynx Global Server 3.0 software (Waters) with an MS tolerance of 5 ppm. Mass analysis of the peptide centroids was performed using DynamX 3.0 software (Waters). Only peptides with scores exceeding 6.4 were considered. The first round of analysis and identification was performed automatically by the DynamX 3.0 software, however, all peptides (deuterated and non-deuterated) were manually verified at every time point for the correct charge state, presence of overlapping peptides, and correct retention time. Deuterium incorporation was not corrected for back-exchange and represents relative, rather than absolute changes in deuterium levels. Changes in H/D amide exchange in any peptide may be due to a single amide or a number of amides within that peptide. The DynamX 3.0 software plots the standard deviation for every peptide. The error band shows the standard deviation of the plotted uptake or difference for each peptide. When there are multiple exposures, as in this experiment, for a given peptide, the maximum standard deviation is plotted for each peptide. A sigma multiplier of 1 is applied to the standard deviation to produce the grey error bar plotted in Extended Data Fig. 7b-e.

Data Availability. The cryo-EM maps and the refined atomic model of *Dm*SERINC were deposited in the EMDB and wwPDB, respectively, with accession codes EMD-10277 and EMD-10279 and PDB 6SP2. Source data for Figures 4a, 4b, 4c, 4e and for Extended Data Figures 1a, 1c, 1d, 1e, 2b, 3b, 4g-i, 6e-g, are available with the paper online.

References

32. Bell, J.M., Chen, M., Baldwin, P.R. & Ludtke, S.J. High resolution single particle refinement in EMAN2.1. *Methods* **100**, 25-34 (2016).

33. Scheres, S.H. RELION: implementation of a Bayesian approach to cryo-EM structure determination. *J Struct Biol* **180**, 519-30 (2012).

34. Punjani, A., Rubinstein, J.L., Fleet, D.J. & Brubaker, M.A. cryoSPARC: algorithms for rapid unsupervised cryo-EM structure determination. *Nat Methods* **14**, 290-296 (2017).

35. Zheng, S.Q. et al. MotionCor2: anisotropic correction of beam-induced motion for improved cryo-electron microscopy. *Nat Methods* **14**, 331-332 (2017).

36. Zhang, K. Gctf: Real-time CTF determination and correction. *J Struct Biol* **193**, 1-12 (2016).

37. Scheres, S.H. & Chen, S. Prevention of overfitting in cryo-EM structure determination. *Nat Methods* **9**, 853-4 (2012).

38. Heymann, J.B. & Belnap, D.M. Bsoft: image processing and molecular modeling for electron microscopy. *J Struct Biol* **157**, 3-18 (2007).

39. Emsley, P. & Cowtan, K. Coot: model-building tools for molecular graphics. *Acta Crystallogr D Biol Crystallogr* **60**, 2126-32 (2004).

40. Afonine, P.V. et al. Real-space refinement in PHENIX for cryo-EM and crystallography. *Acta Crystallogr D Struct Biol* **74**, 531-544 (2018).

41. Adams, P.D. et al. PHENIX: a comprehensive Python-based system for macromolecular structure solution. *Acta Crystallogr D Biol Crystallogr* **66**, 213-21 (2010).

42. Chen, V.B. et al. MolProbity: all-atom structure validation for macromolecular crystallography. *Acta Crystallogr D Biol Crystallogr* **66**, 12-21 (2010).

43. Barad, B.A. et al. EMRinger: side chain-directed model and map validation for 3D cryo-electron microscopy. *Nat Methods* **12**, 943-6 (2015).

44. Waterhouse, A. et al. SWISS-MODEL: homology modelling of protein structures and complexes. *Nucleic Acids Res* **46**, W296-W303 (2018).

45. Krissinel, E. & Henrick, K. Inference of macromolecular assemblies from crystalline state. *J Mol Biol* **372**, 774-97 (2007).

46. Lomize, M.A., Pogozheva, I.D., Joo, H., Mosberg, H.I. & Lomize, A.L. OPM database and PPM web server: resources for positioning of proteins in membranes. *Nucleic Acids Res* **40**, D370-6 (2012).

47. Marrink, S.J., Risselada, H.J., Yefimov, S., Tieleman, D.P. & de Vries, A.H. The MARTINI force field: coarse grained model for biomolecular simulations. *J Phys Chem B* **111**, 7812-24 (2007).

48. Monticelli, L. et al. The MARTINI Coarse-Grained Force Field: Extension to Proteins. *J Chem Theory Comput* **4**, 819-34 (2008).

49. Stansfeld, P.J. & Sansom, M.S. From Coarse Grained to Atomistic: A Serial Multiscale Approach to Membrane Protein Simulations. *J Chem Theory Comput* **7**, 1157-66 (2011).

50. Huang, J. & MacKerell, A.D., Jr. CHARMM36 all-atom additive protein force field: validation based on comparison to NMR data. *J Comput Chem* **34**, 2135-45 (2013).

51. Olesen, K., Awasthi, N., Bruhn, D.S., Pezeshkian, W. & Khandelia, H. Faster Simulations with a 5 fs Time Step for Lipids in the CHARMM Force Field. *J Chem Theory Comput* **14**, 3342-3350 (2018).

52. Berendsen, H.J.C., van der Spoel, D. & van Drunen, R. GROMACS: A message-passing parallel molecular dynamics implementation. *Comput Phys Commun* **91**, 43-56 (1995).

53. Humphrey, W., Dalke, A. & Schulten, K. VMD: Visual molecular dynamics *J Mol Graph* **14**, 33-8 (1996).

54. Pizzato, M. et al. A one-step SYBR Green I-based product-enhanced reverse transcriptase assay for the quantitation of retroviruses in cell culture supernatants. *J Virol Methods* **156**, 1-7 (2009).

55. Gault, J. et al. High-resolution mass spectrometry of small molecules bound to membrane proteins. *Nat Methods* **13**, 333-6 (2016).

56. Hernandez, H. & Robinson, C.V. Determining the stoichiometry and interactions of macromolecular assemblies from mass spectrometry. *Nat Protoc* **2**, 715-26 (2007).

57. Marty, M.T. et al. Bayesian deconvolution of mass and ion mobility spectra: from binary interactions to polydisperse ensembles. *Anal Chem* **87**, 4370-6 (2015).

58. Silva, J.C. et al. Quantitative proteomic analysis by accurate mass retention time pairs. *Anal Chem* **77**, 2187-200 (2005).

59. Frigola, J., Remus, D., Mehanna, A. & Diffley, J.F. ATPase-dependent quality control of DNA replication origin licensing. *Nature* **495**, 339-43 (2013).

60. Ulm, J.W., Perron, M., Sodroski, J. & R, C.M. Complex determinants within the Moloney murine leukemia virus capsid modulate susceptibility of the virus to Fv1 and Ref1-mediated restriction. *Virology* **363**, 245-55 (2007).

61. Robert, X. & Gouet, P. Deciphering key features in protein structures with the new ENDscript server. *Nucleic Acids Res* **42**, W320-4 (2014).

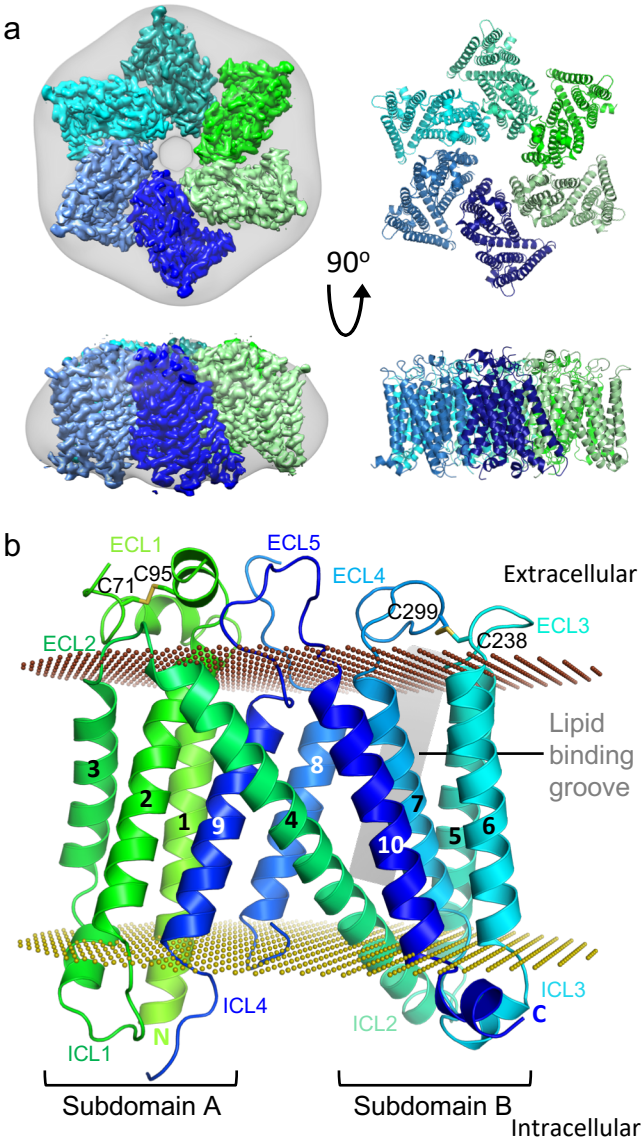
a
90º
b
ECL1
ECL5
ECL4
Extracellular
C71
C95
C299
ECL3
C238
ECL2
Lipid
binding
groove
3
2
1
9
8
4
7
10
5
6
ICL4
ICL3
ICL2
C
N
ICL1
Subdomain A
Subdomain B
Intracellular

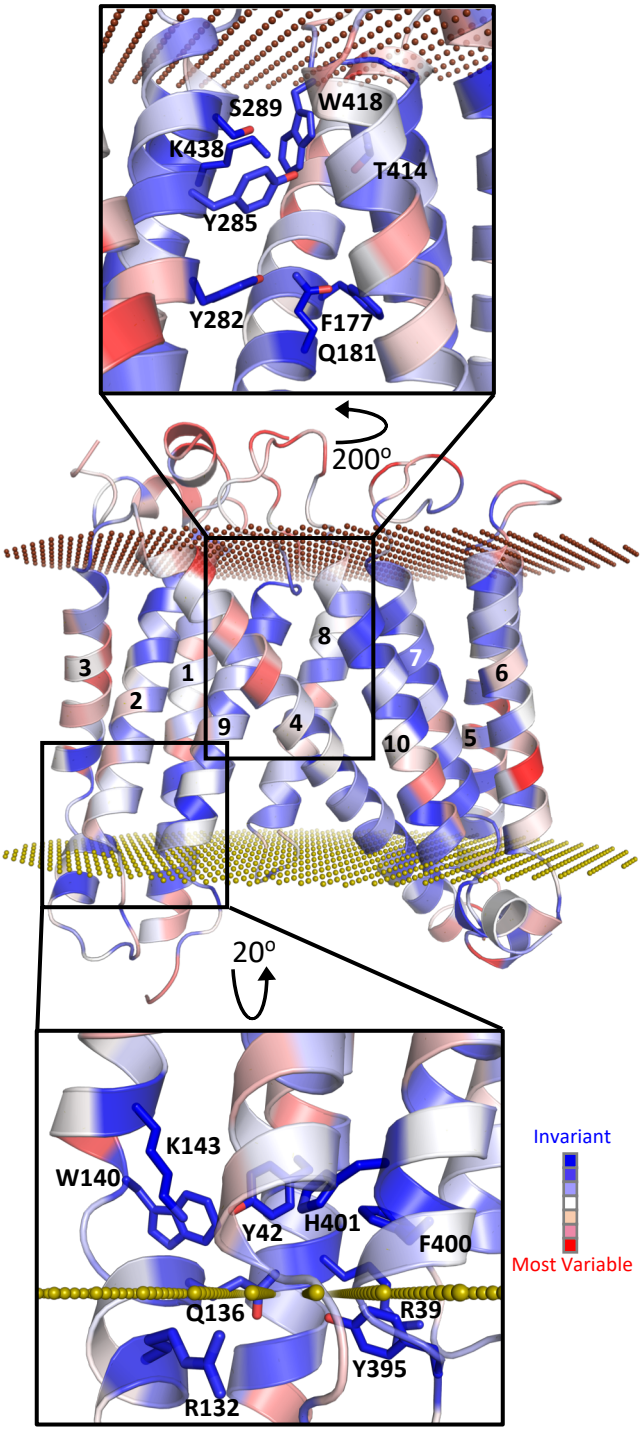
S289
W418
K438
T414
Y285
Y282
F177
Q181
200°
3
1
2
9
4
8
7
10
6
5
20°
K143
W140
Y42
H401
F400
Q136
R39
Y395
R132
Invariant
Most Variable

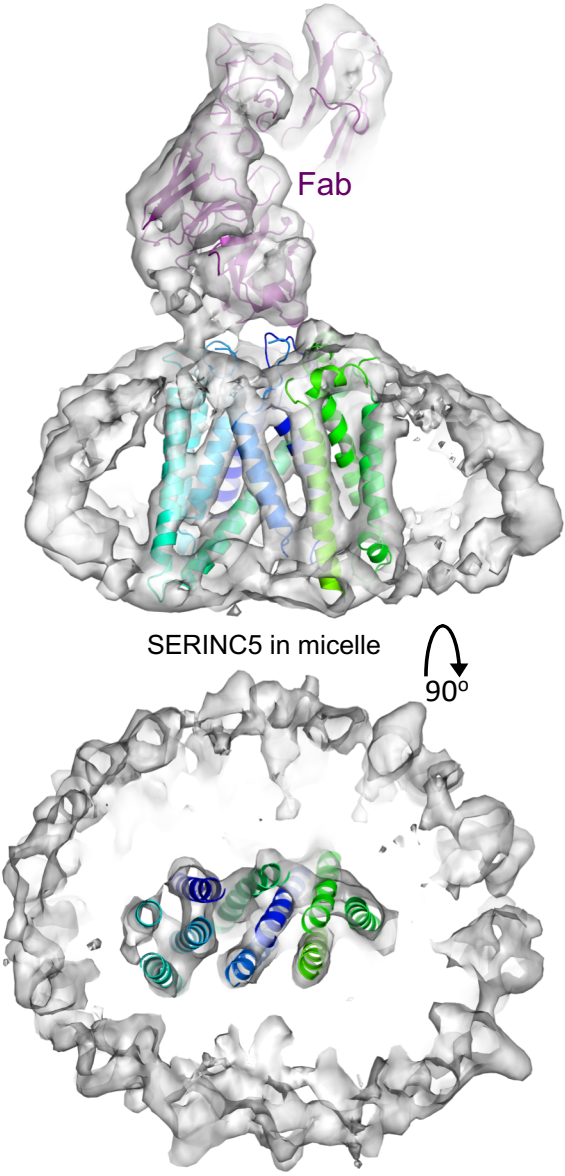
Fab
SERINC5 in micelle
90°

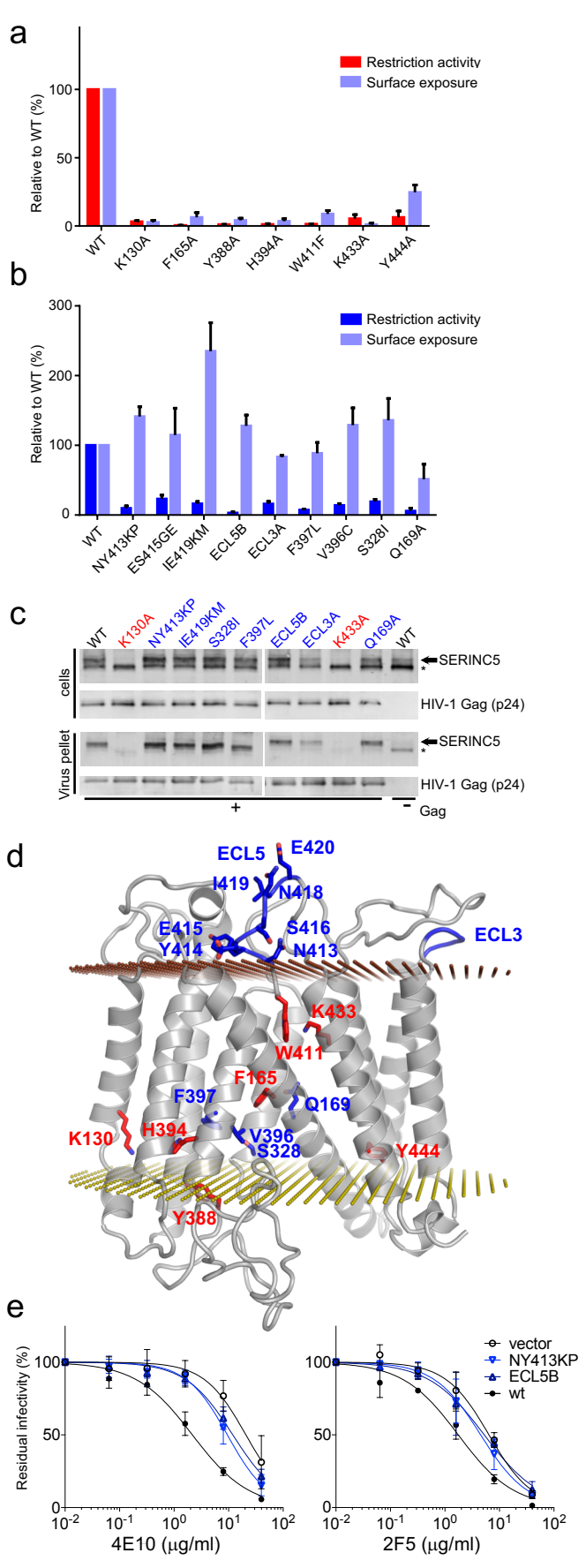
a
Restriction activity
Surface exposure
Relative to WT (%)
100
50
0
WT
K130A
F165A
Y388A
H394A
W411F
K433A
Y444A
b
Restriction activity
Surface exposure
Relative to WT (%)
300
200
100
0
WT
NY413KP
ES415GE
IE419KM
ECL5B
ECL3A
F397L
V396C
S328I
Q169A
c
WT
K130A
NY413KP
IE419KM
S328I
F397L
ECL5B
ECL3A
K433A
Q169A
WT
cells
SERINC5
HIV-1 Gag (p24)
Virus pellet
SERINC5
HIV-1 Gag (p24)
+
-
Gag
d
ECL5
E420
I419
N418
E415
S416
Y414
N413
ECL3
K433
W411
F165
F397
Q169
K130
H394
V396
S328
Y444
Y388
e
vector
NY413KP
ECL5B
wt
Residual infectivity (%)
100
50
0
10^{-2}
10^{-1}
10^{0}
10^{1}
10^{2}
4E10 (μg/ml)
2F5 (μg/ml)

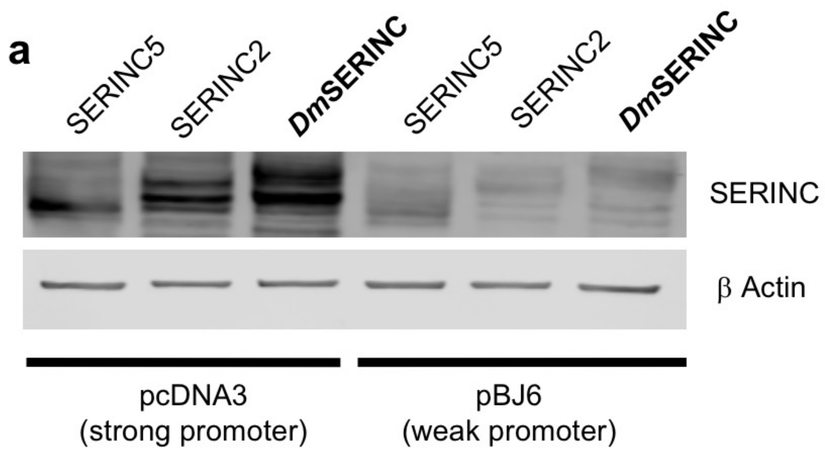
a
SERINC5
SERINC2
DmSERINC
SERINC5
SERINC2
DmSERINC
SERINC
β Actin
pcDNA3
(strong promoter)
pBJ6
(weak promoter)

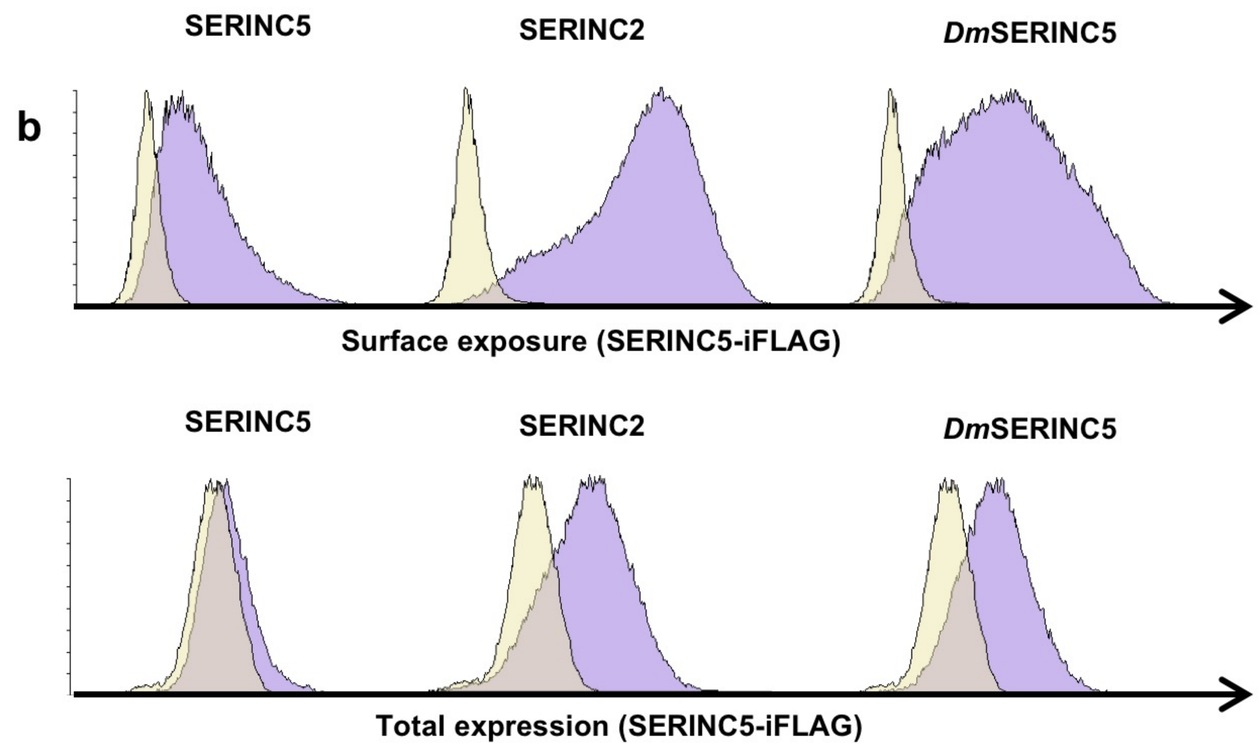
b
SERINC5
SERINC2
DmSERINC5
Surface exposure (SERINC5-iFLAG)
SERINC5
SERINC2
DmSERINC5
Total expression (SERINC5-iFLAG)

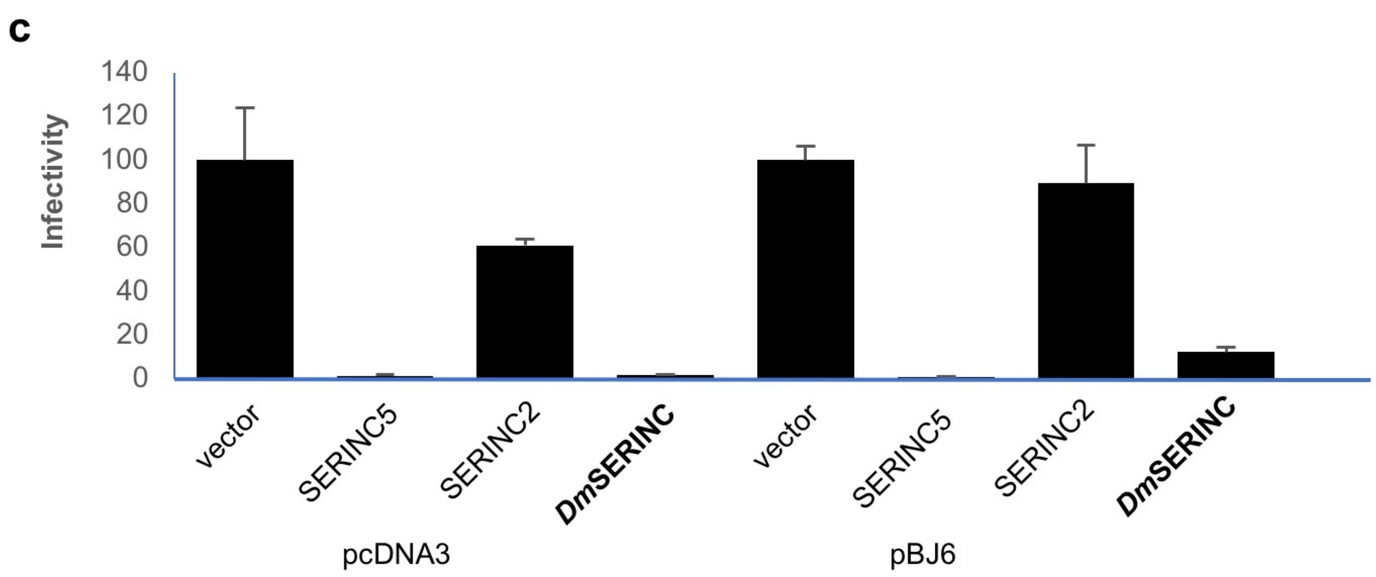
c
Infectivity
140
120
100
80
60
40
20
0
vector
SERINC5
SERINC2
DmSERINC
vector
SERINC5
SERINC2
DmSERINC
pcDNA3
pBJ6

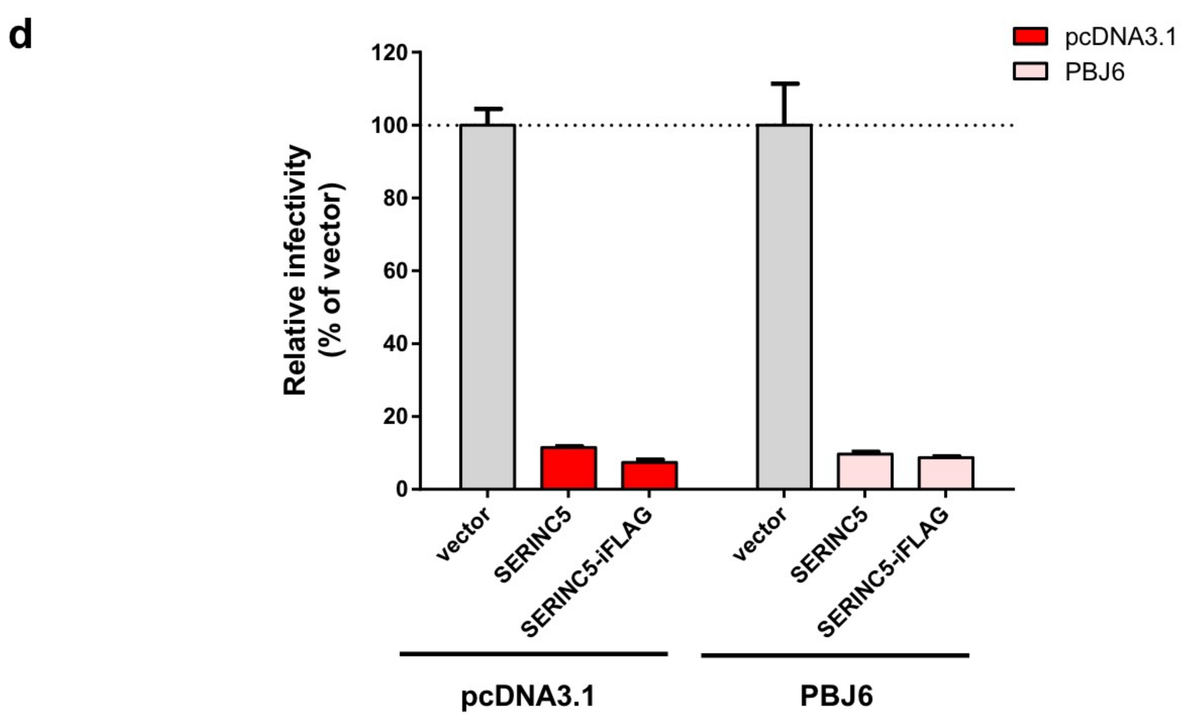
d
pcDNA3.1
PBJ6
Relative infectivity
(% of vector)
120
100
80
60
40
20
0
vector
SERINC5
SERINC5-iFLAG
vector
SERINC5
SERINC5-iFLAG
pcDNA3.1
PBJ6

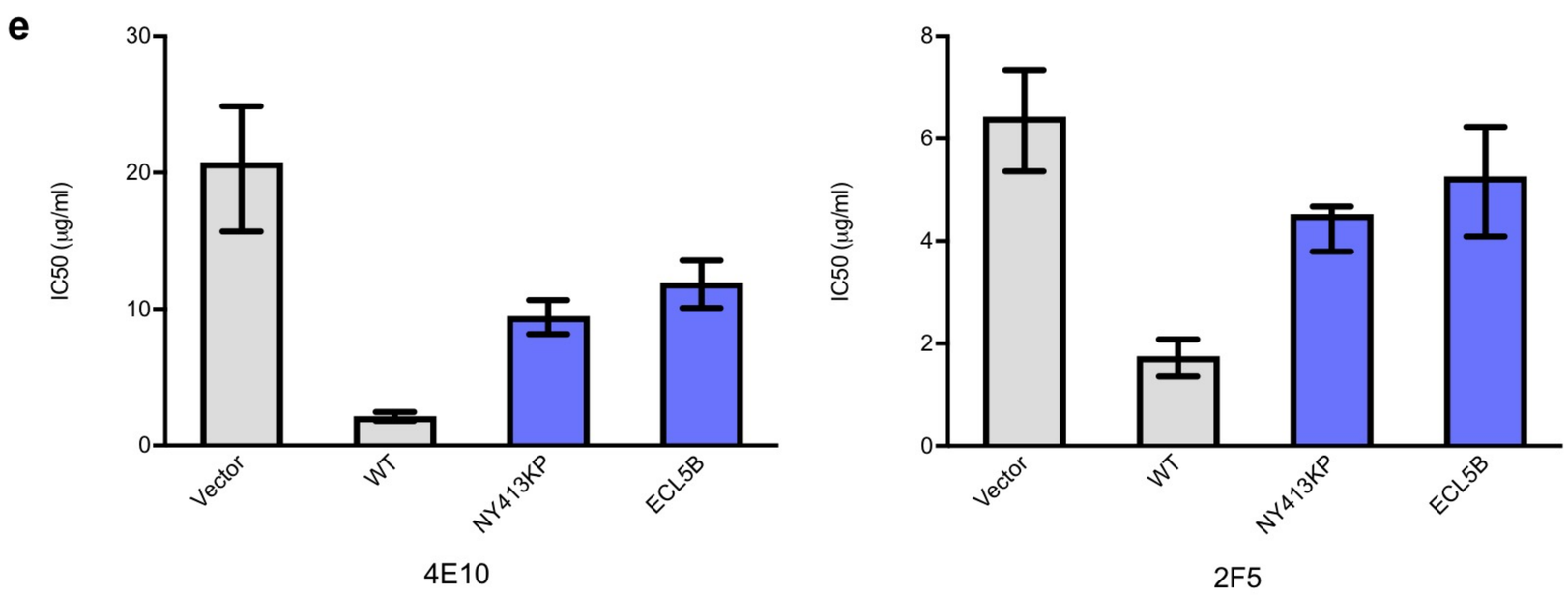
e
IC50 (μg/ml)
30
20
10
0
Vector
WT
NY413KP
ECL5B
4E10
IC50 (μg/ml)
8
6
4
2
0
Vector
WT
NY413KP
ECL5B
2F5

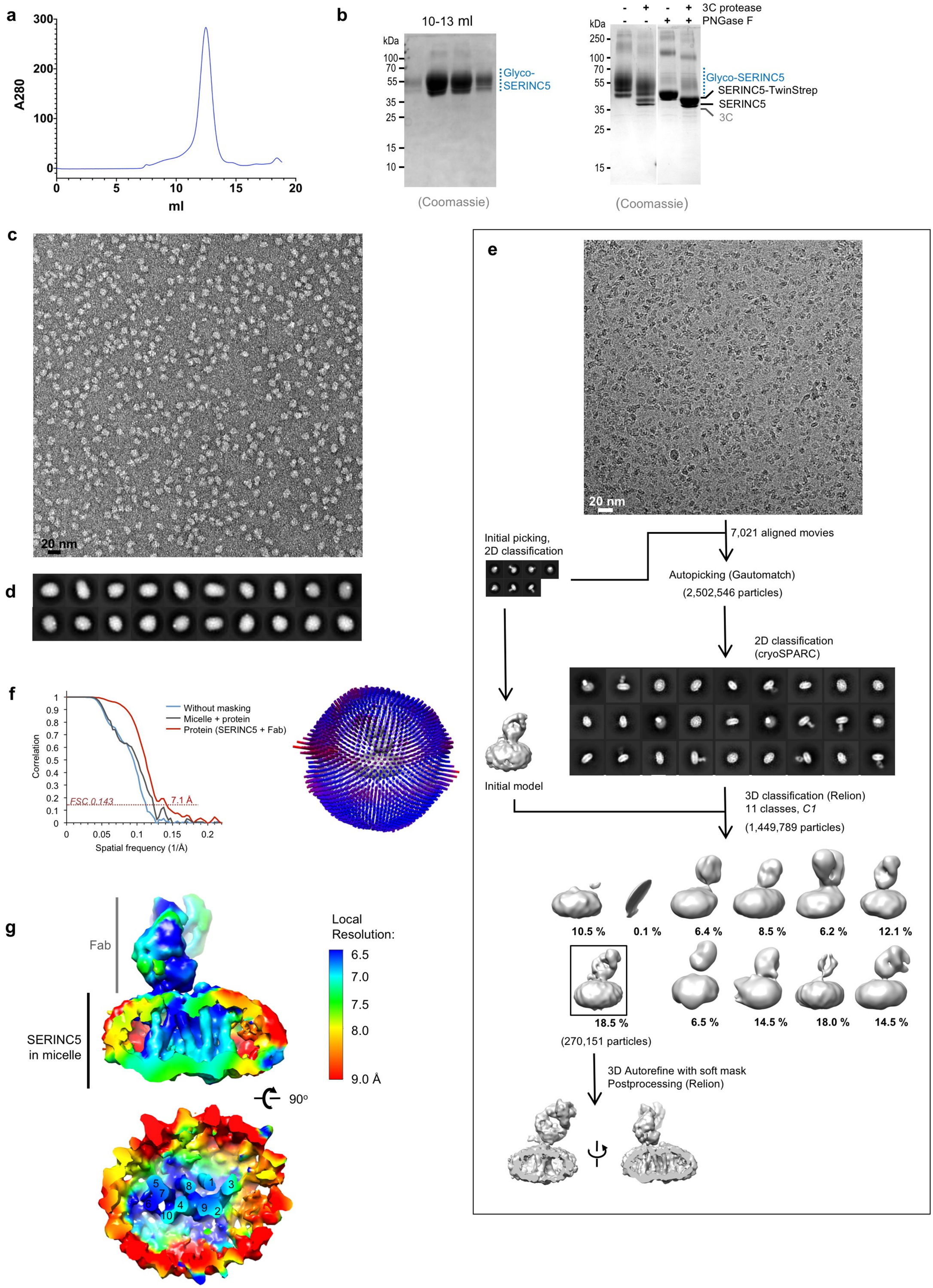
a
A280
ml
b
10-13 ml
kDa
Glyco-SERINC5
(Coomassie)
3C protease
PNGase F
Glyco-SERINC5
SERINC5-TwinStrep
SERINC5
3C
(Coomassie)
c
20 nm
d
e
20 nm
Initial picking, 2D classification
7,021 aligned movies
Autopicking (Gautomatch)
(2,502,546 particles)
2D classification (cryoSPARC)
Initial model
3D classification (Relion)
11 classes, C1
(1,449,789 particles)
10.5 %
0.1 %
6.4 %
8.5 %
6.2 %
12.1 %
18.5 %
6.5 %
14.5 %
18.0 %
14.5 %
(270,151 particles)
3D Autorefine with soft mask
Postprocessing (Relion)
f
Correlation
Spatial frequency (1/Å)
Without masking
Micelle + protein
Protein (SERINC5 + Fab)
FSC 0.143
7.1 Å
g
Fab
SERINC5 in micelle
Local Resolution:
6.5
7.0
7.5
8.0
9.0 Å
90°

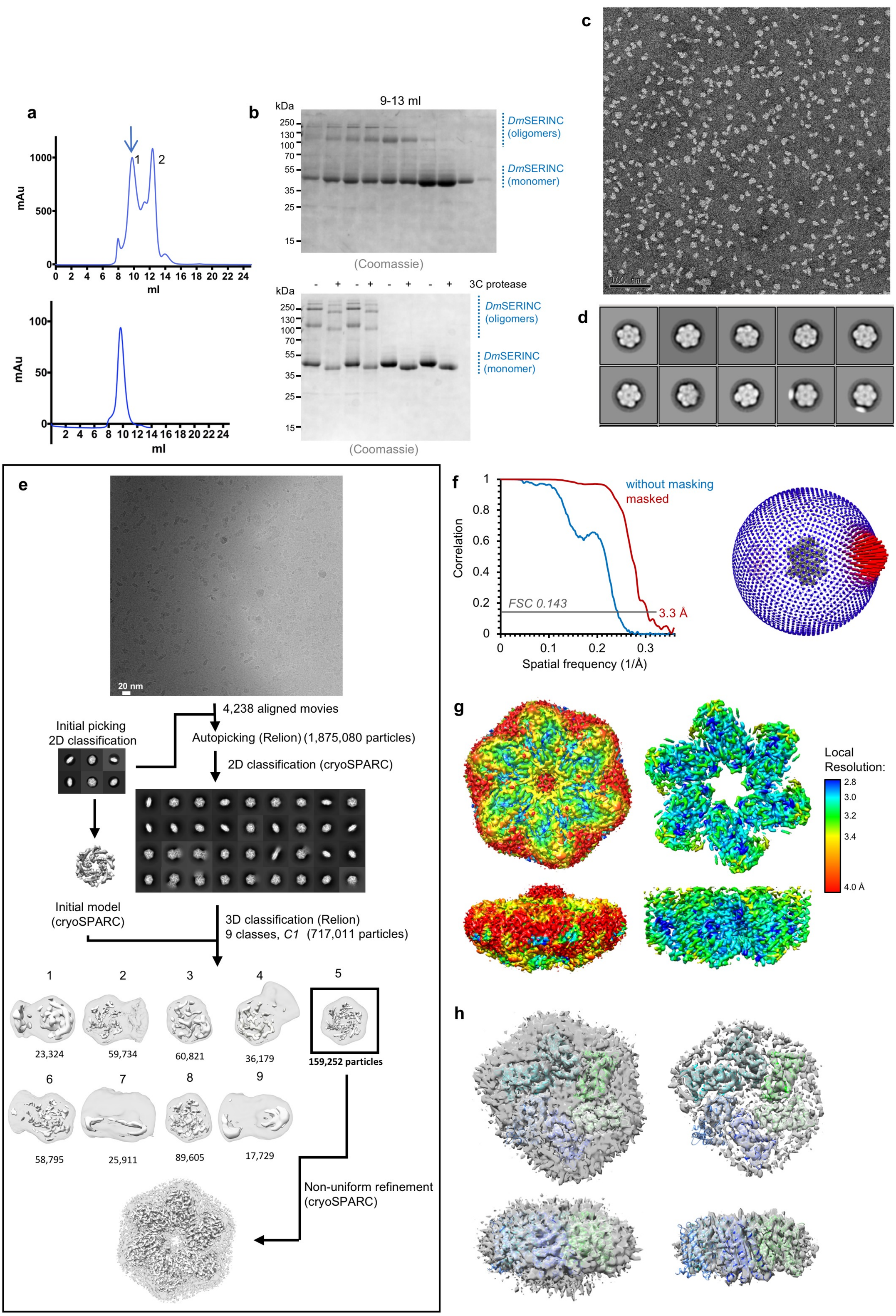
a
mAu
ml
1
2
b
9-13 ml
kDa
DmSERINC (oligomers)
DmSERINC (monomer)
(Coomassie)
3C protease
c
100 nm
d
e
20 nm
4,238 aligned movies
Initial picking
2D classification
Autopicking (Relion) (1,875,080 particles)
2D classification (cryoSPARC)
Initial model (cryoSPARC)
3D classification (Relion)
9 classes, C1 (717,011 particles)
23,324
59,734
60,821
36,179
159,252 particles
58,795
25,911
89,605
17,729
Non-uniform refinement (cryoSPARC)
f
Correlation
without masking
masked
FSC 0.143
3.3 Å
Spatial frequency (1/Å)
g
Local Resolution:
2.8
3.0
3.2
3.4
4.0 Å
h

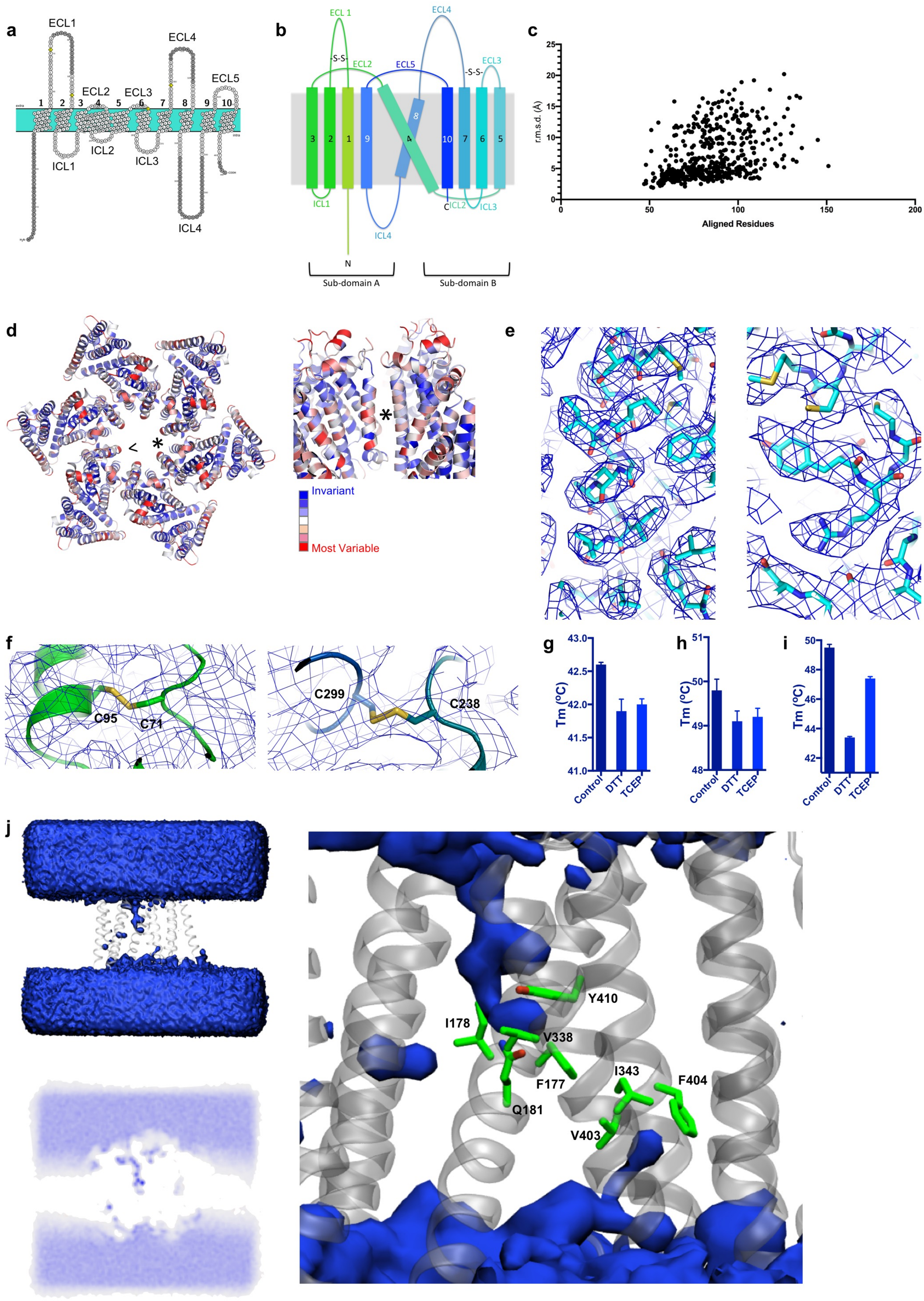
a
ECL1
ECL4
ECL5
ECL2
ECL3
1 2 3 4 5 6 7 8 9 10
ICL1
ICL2
ICL3
ICL4
b
ECL 1
ECL4
-S-S-
ECL2
ECL5
-S-S-
ECL3
3 2 1 9 8 10 7 6 5
ICL1
ICL4
C
ICL2
ICL3
N
Sub-domain A
Sub-domain B
c
r.m.s.d. (Å)
Aligned Residues
d
Invariant
Most Variable
e
f
C95
C71
C299
C238
g
h
i
Tm (°C)
Control
DTT
TCEP
j
Y410
I178
V338
F177
Q181
I343
F404
V403

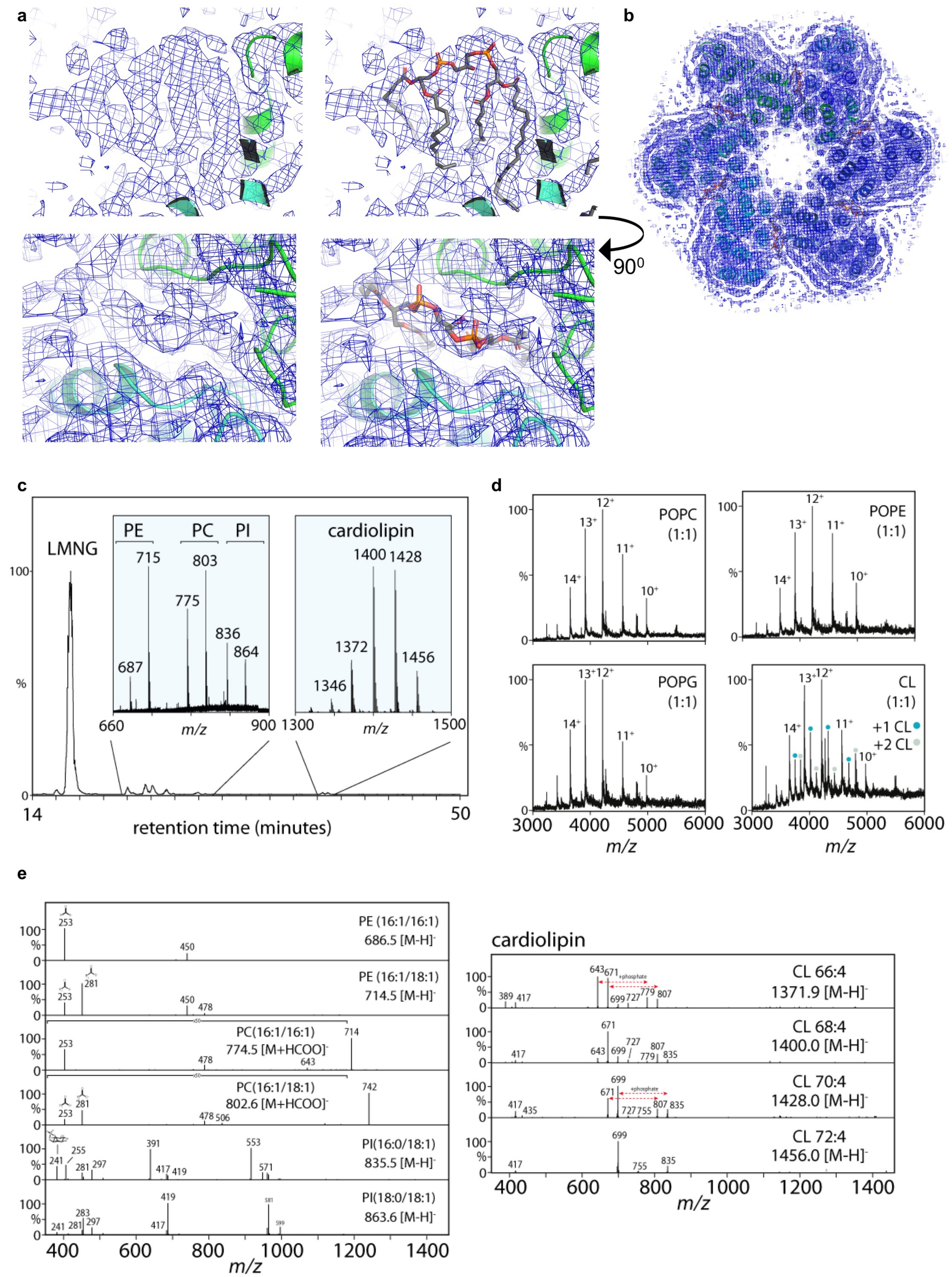
a
b
90⁰
c
LMNG
PE
PC
PI
715
803
775
836
864
687
cardiolipin
1400
1428
1372
1456
1346
660
m/z
900
1300
1500
100
%
0
14
50
retention time (minutes)
d
POPC
(1:1)
POPE
(1:1)
POPG
(1:1)
CL
(1:1)
+1 CL
+2 CL
14+
13+
12+
11+
10+
3000
4000
5000
6000
e
PE (16:1/16:1)
686.5 [M-H]-
PE (16:1/18:1)
714.5 [M-H]-
PC(16:1/16:1)
774.5 [M+HCOO]-
PC(16:1/18:1)
802.6 [M+HCOO]-
PI(16:0/18:1)
835.5 [M-H]-
PI(18:0/18:1)
863.6 [M-H]-
cardiolipin
CL 66:4
1371.9 [M-H]-
CL 68:4
1400.0 [M-H]-
CL 70:4
1428.0 [M-H]-
CL 72:4
1456.0 [M-H]-
+phosphate
400
600
800
1000
1200
1400

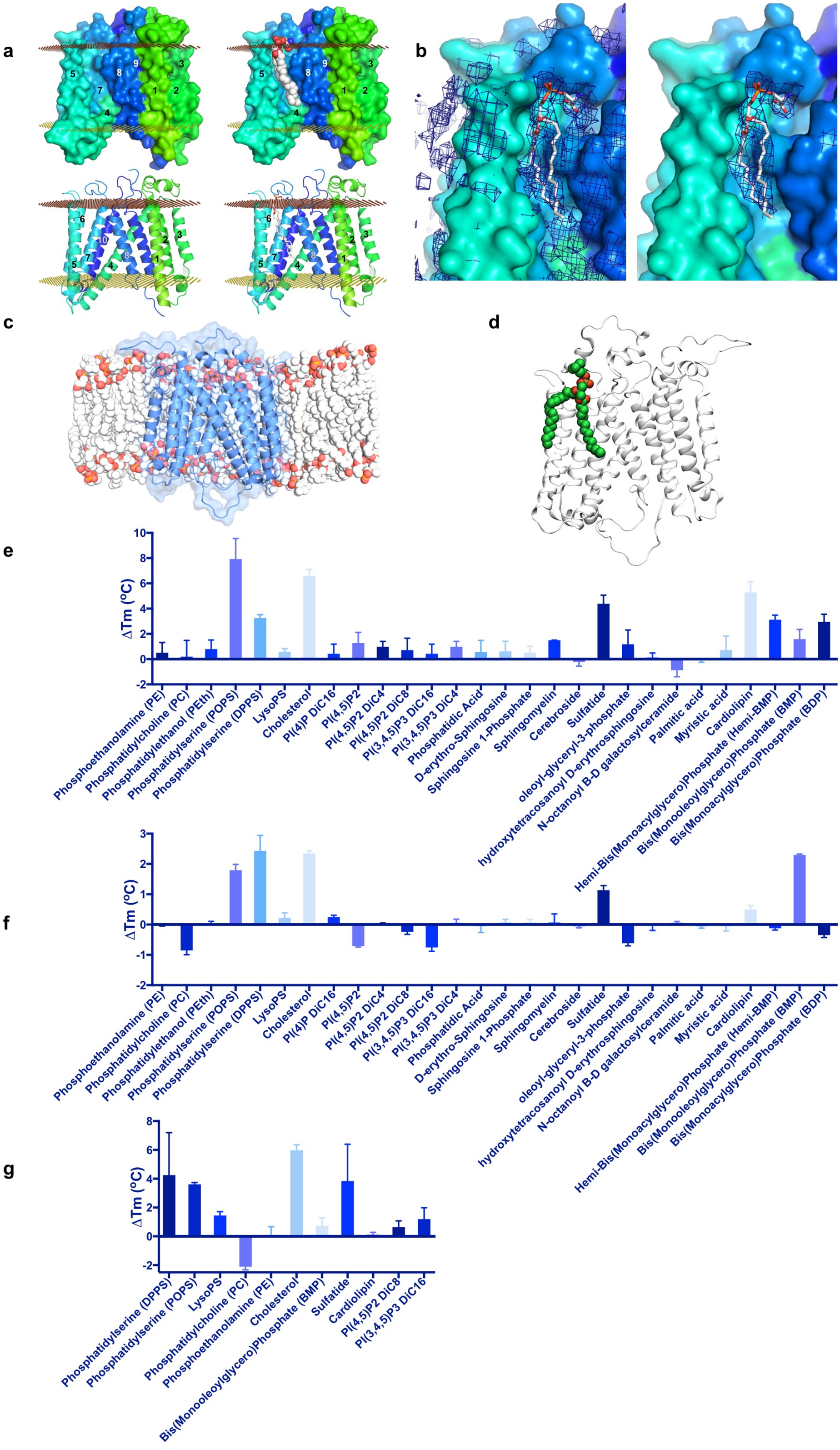
a
b
c
d
e
f
g
ΔTm (ºC)
Phosphoethanolamine (PE)
Phosphatidylcholine (PC)
Phosphatidylethanol (PEth)
Phosphatidylserine (POPS)
Phosphatidylserine (DPPS)
LysoPS
Cholesterol
PI(4)P DiC16
PI(4,5)P2
PI(4,5)P2 DiC4
PI(4,5)P2 DiC8
PI(3,4,5)P3 DiC16
PI(3,4,5)P3 DiC4
Phosphatidic Acid
D-erythro-Sphingosine
Sphingosine 1-Phosphate
Sphingomyelin
Cerebroside
Sulfatide
oleoyl-glyceryl-3-phosphate
hydroxytetracosanoyl D-erythrosphingosine
N-octanoyl B-D galactosylceramide
Palmitic acid
Myristic acid
Cardiolipin
Hemi-Bis(Monoacylglycero)Phosphate (Hemi-BMP)
Bis(Monooleoylglycero)Phosphate (BMP)
Bis(Monoacylglycero)Phosphate (BDP)

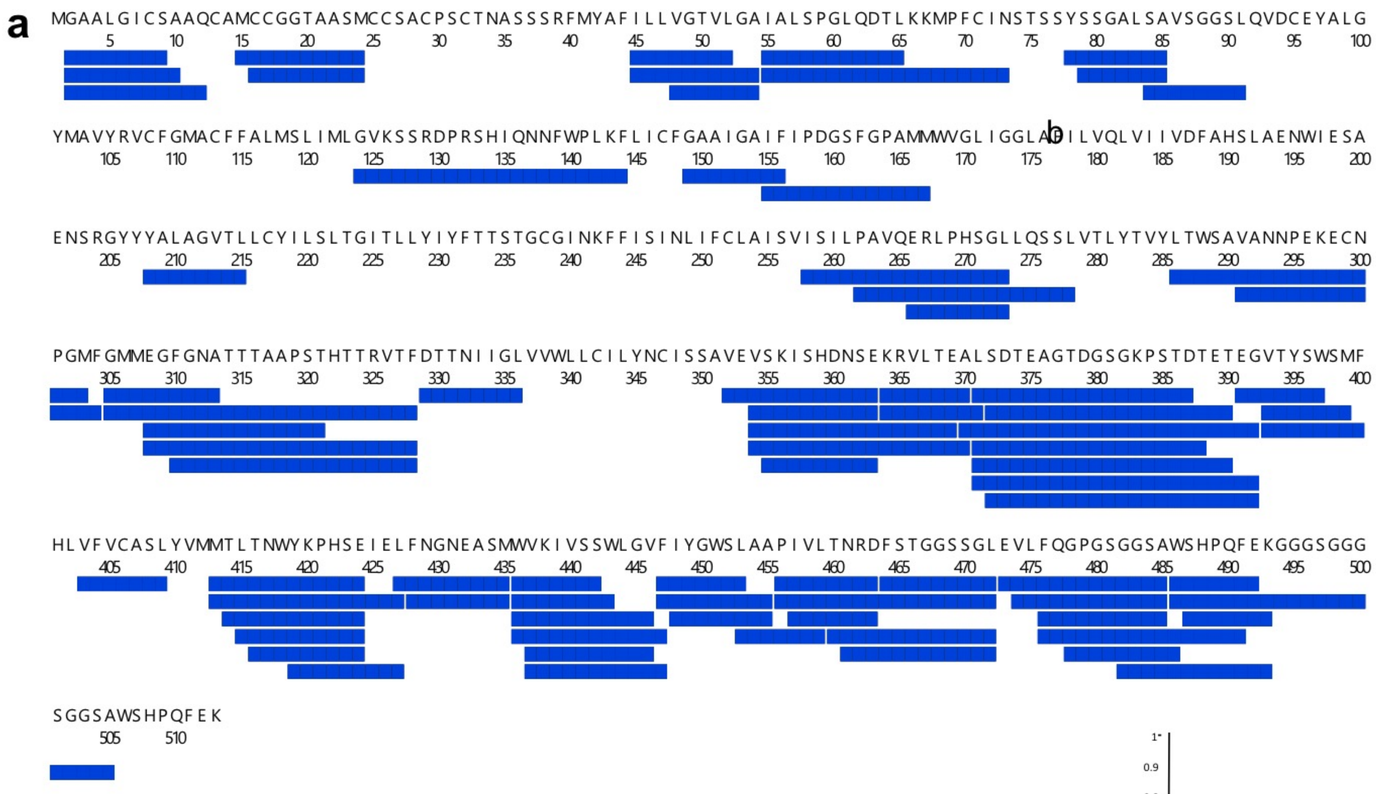

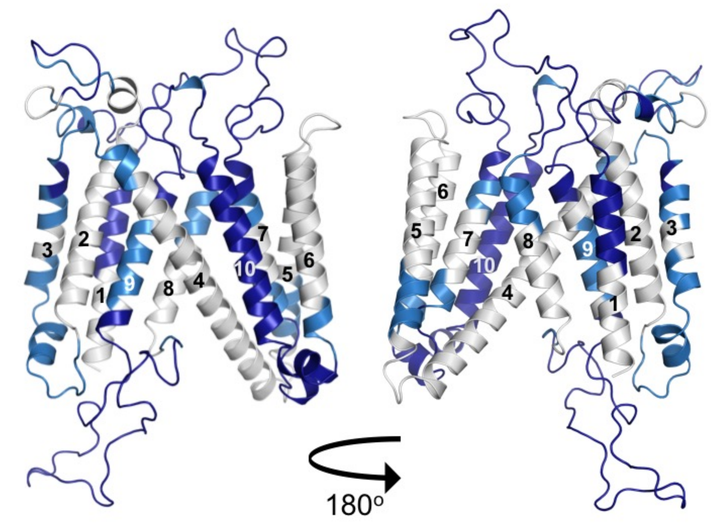

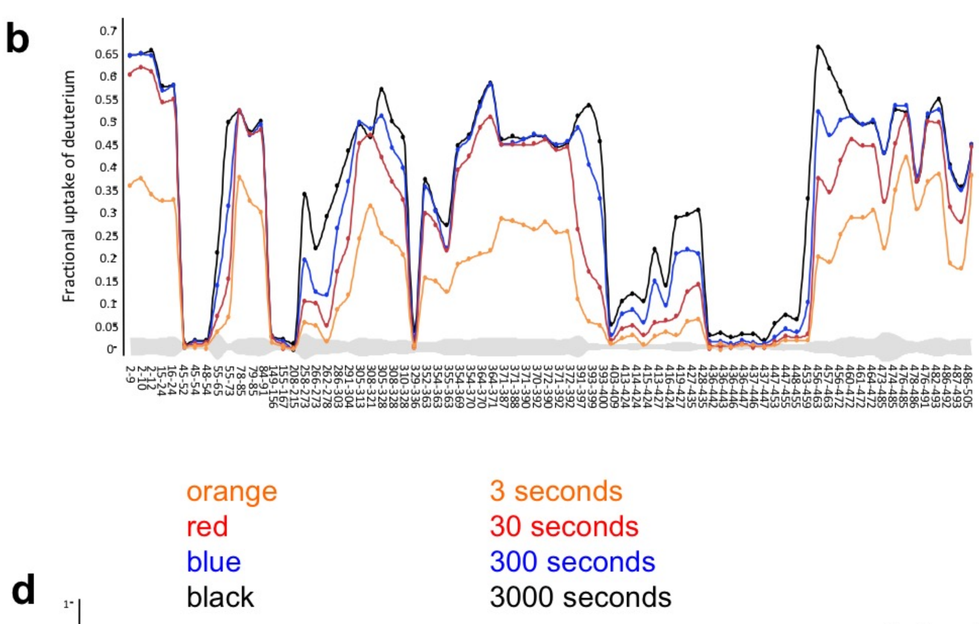

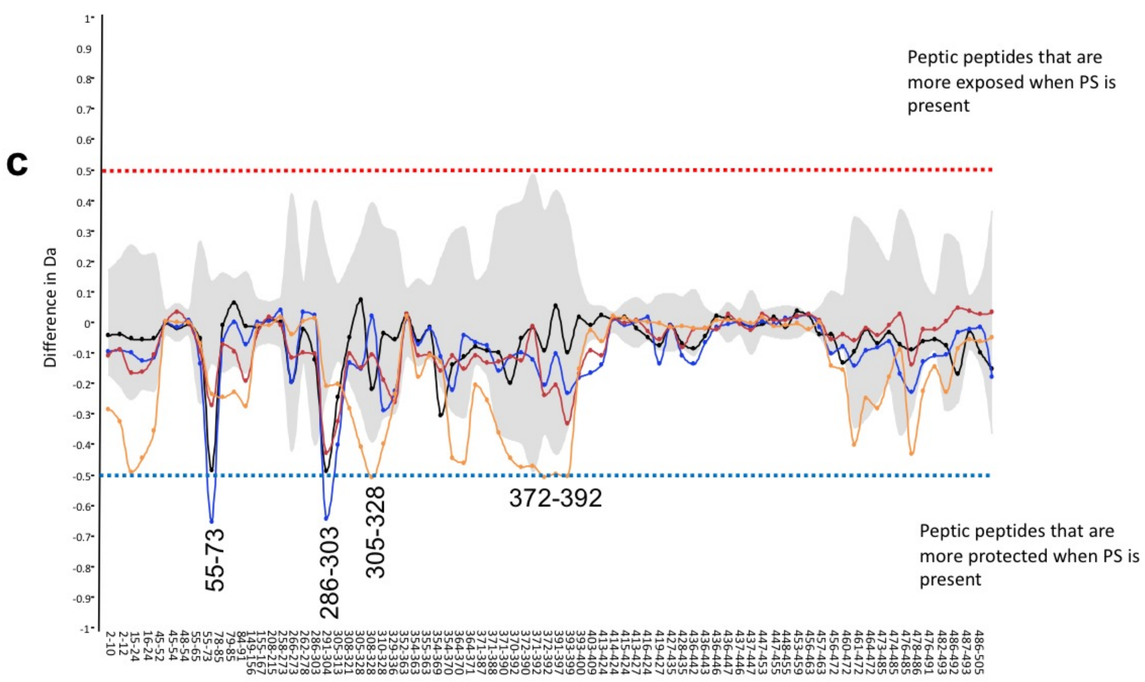

orange 3 seconds
red 30 seconds
blue 300 seconds
black 3000 seconds

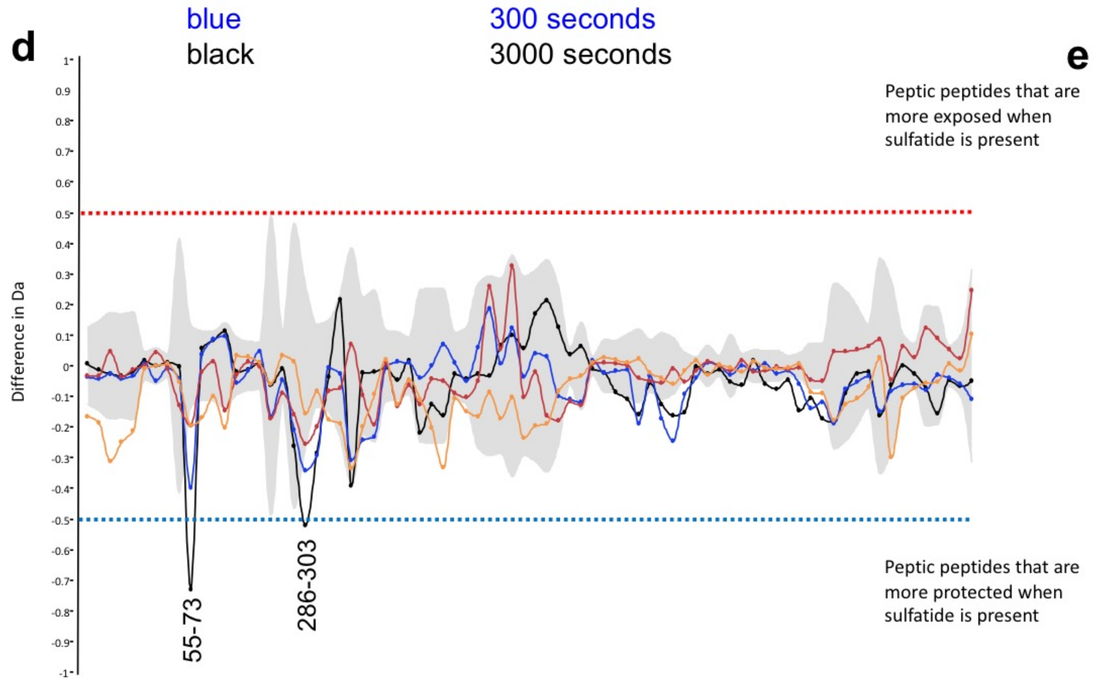

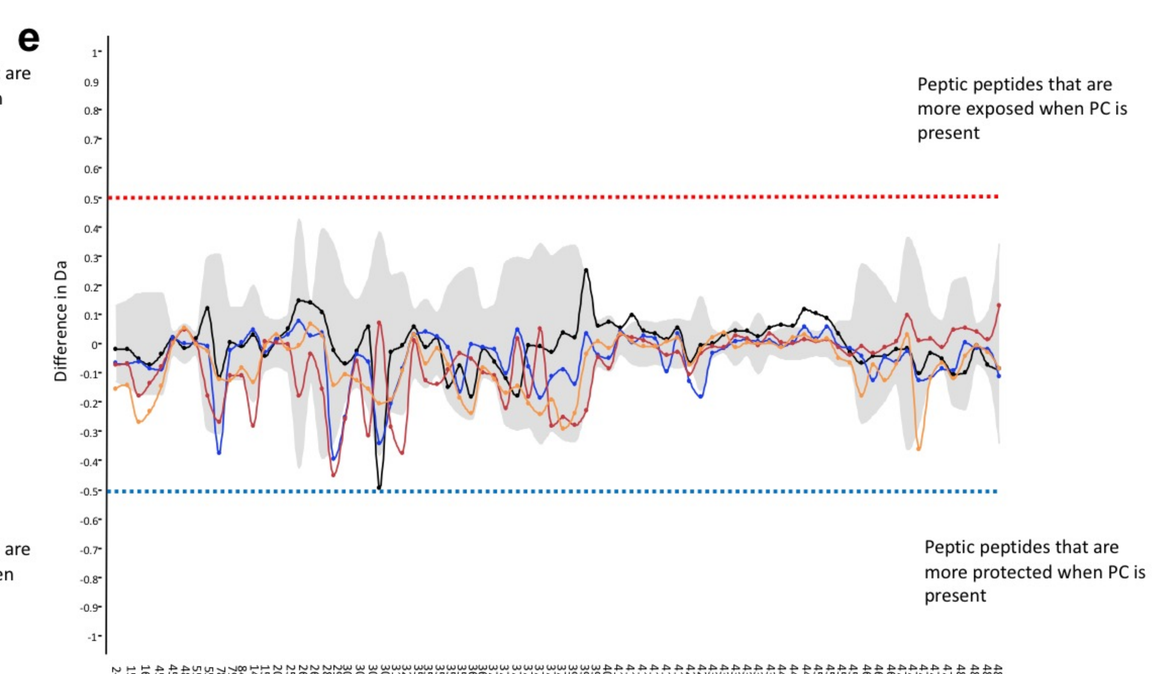

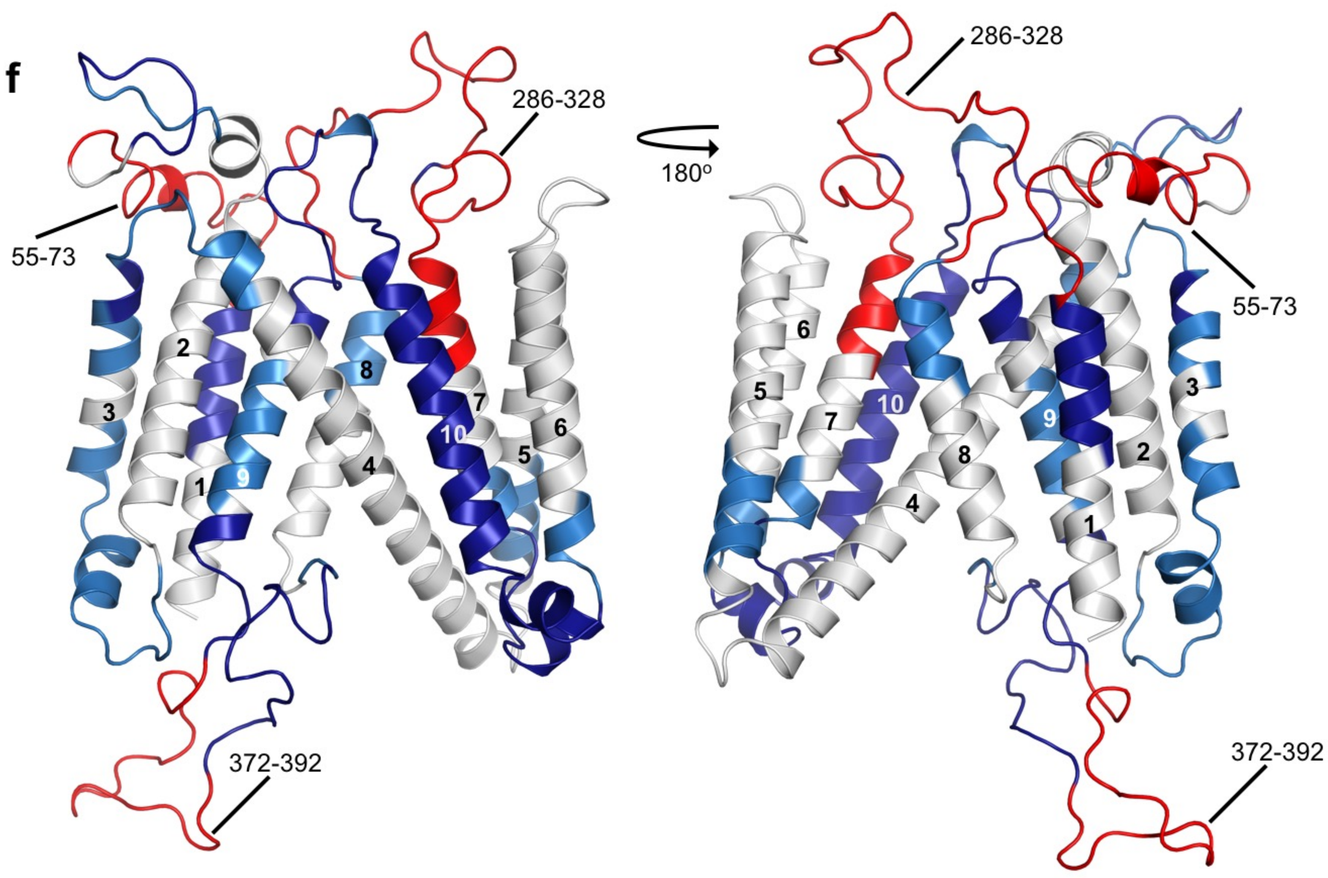

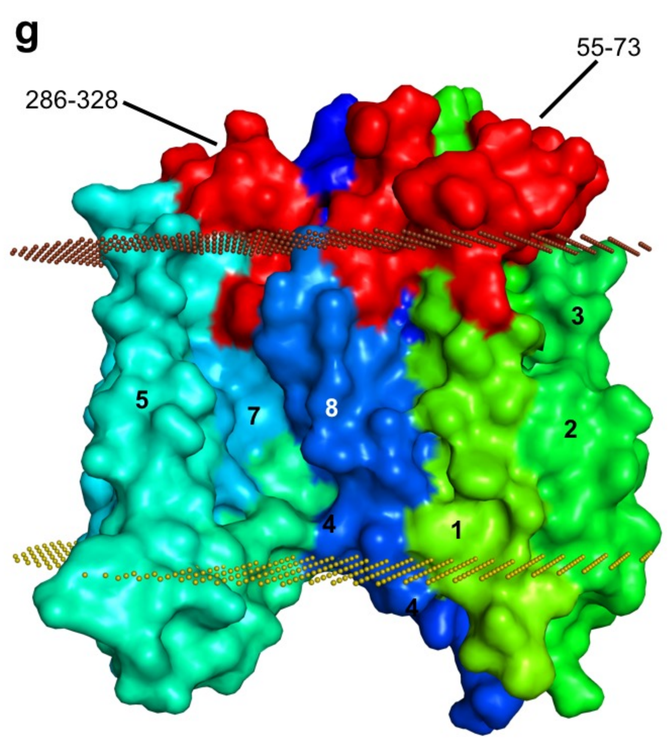

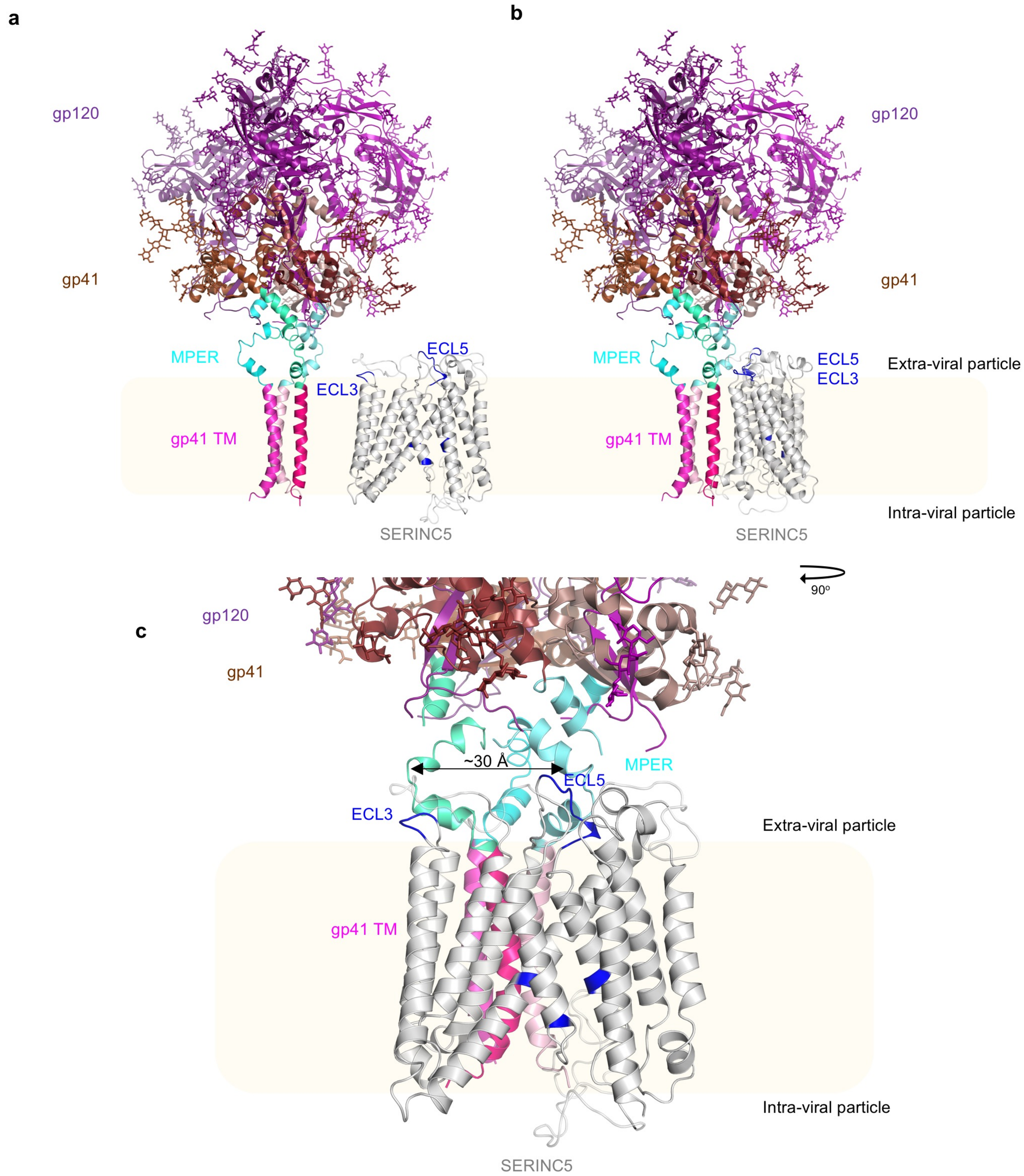
a
gp120
gp41
MPER
ECL5
ECL3
gp41 TM
SERINC5
b
gp120
gp41
MPER
ECL5
ECL3
Extra-viral particle
gp41 TM
Intra-viral particle
SERINC5
90°
c
gp120
gp41
~30 Å
MPER
ECL5
ECL3
Extra-viral particle
gp41 TM
Intra-viral particle
SERINC5